Instability of Flow In Magnetic Nozzle

Hunt Feng

April 25, 2024

Contents

Abstract

Spectral method is a common technique for analyzing the instability of a dynamical system. By discretizing the linearized equations motion of magnetic nozzle, the instability problem becomes a polynomial eigenvalue problem. Given Dirichlet boundary condition, we found that the flow with subsonic and supersonic velocity profiles are stable. Given fixed-open boundary condition, the subsonic flow is stable, but the supersonic flow is unstable. Different discretizations, such as finite difference, finite element and spectral element method agree with each other. By studying the convergence of different modes, we successfully eliminated the spurious unstable modes.

However, spectral method is not enough to analyze the full problem. The problem has a singularity at the throat of the nozzle if the flow is transonic. The existence of singularity prevents the use of spectral method. We then expand the solution at the singularity and found the regular solution. Using that together with shooting method, we are able to solve the polynomial eigenvalue problem. The flow with accelerating velocity profile is stable.

Chapter 1

Introduction

1.1 Plasma

Plasma is often called the fourth state of matter after solid, liquid, and gas. [8] In a plasma, the atoms or molecules have been stripped of electrons, resulting in a collection of charged particles, ions and electrons.

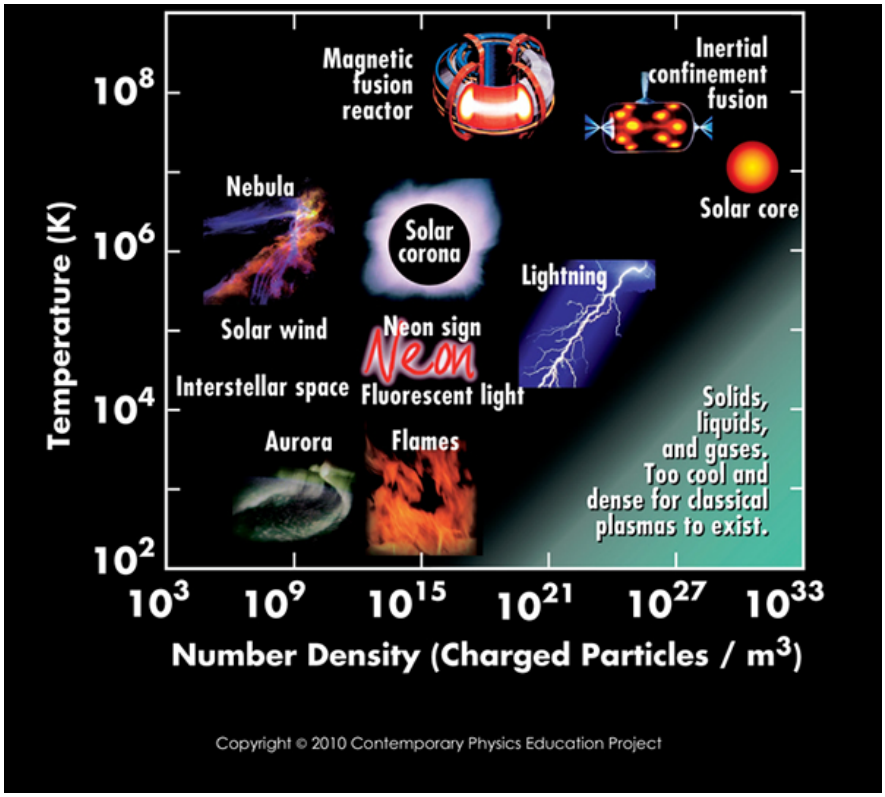

Figure 1.1: Typical plasmas. Adapted from [1]

Plasma is a common state of matter, some examples are listed on Fig. 1.1. Natural

plasmas include nebula, solar wind, aurora, etc. These natural plasmas seen in the sky because they are in plasma state, and plasma is capable of emitting light. [8] Plasma has various scientific and technology uses. The artificially generated plasma can be found in fluorescent lights, Neon signs, etc. It can also be found in plasma physics research, nuclear fusion experiments, plasma cutting and welding, plasma medicine for treating diseases, and even in spacecraft propulsion systems. Overall, plasma is an intriguing and versatile state of matter with significant implications in various fields of science, technology, and industry.

1.1.1 Definition of Plasma

Simply put, a plasma is a quasineutral gas of charged and neutral particles which exhibits collective behavior. [8] Before we give a more precise definition of plasma, some concepts must be introduced.

Debye Shielding and Quasineutrality

A fundamental property of plasma is its ability to shield externally applied electric field. [8] Imagine two balls are connected to a battery, and they are charged. When these charged balls are submerged into a plasma, the ions will surround the positively charged ball, and the electrons will surround the negatively charged ball. See Fig. 1.2. Suppose there are sufficient amounts of ions and electrons in the plasma, and the plasma is cold (no thermal motions) the electric field generated by the two balls will be shielded out by the surrounding ion and electron clouds. If the plasma has finite temperature, then the edge of the cloud occurs at the radius where the potential energy is approximately equal to the thermal energy KT of the particles, and the shielding is not complete.

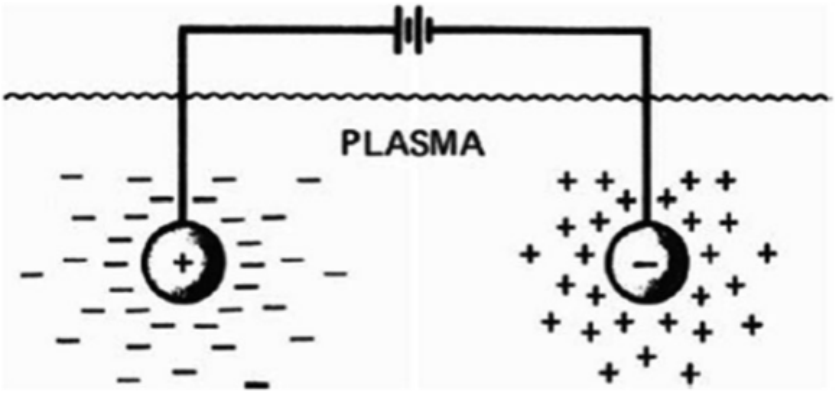

Figure 1.2: Debye shielding. Adapted from [8]. Two charged balls are submerged into a plasma. Ions will surround the positively charged ball, and the electrons will surround the negatively charged ball.

To compute the thickness of the cloud, also known as the Debye length, we focus our view to the positively charged ball. Suppose the coordinate's origin is at the ball's center and $\phi(0) = 0$. We will solve the following 1-dimensional Poisson's equation,

$$\epsilon_0 \frac{\mathrm{d}^2\phi}{\mathrm{d}x^2} = -e(n_i - n_e), \quad \phi(0) = \phi_0 \tag{1.1}$$

where n is the number density of the particles, and the subscripts i and e stand for ion and electron.

For simplicity, we assume massless electron, $m/M \to 0$. The solution to the Poisson's equation is

$$\phi = \phi_0 \exp(-|x|/\lambda_D) \tag{1.2}$$

where the quantity λ_D is called Debye length, and is defined as

$$\lambda_D \equiv \left(\frac{\epsilon_0 KT}{ne^2}\right)^{1/2} \tag{1.3}$$

where n stands for the number density far away from the charged ball. The potential is shown in Fig. 1.3. The Debye length characterizes the thickness the of the cloud.

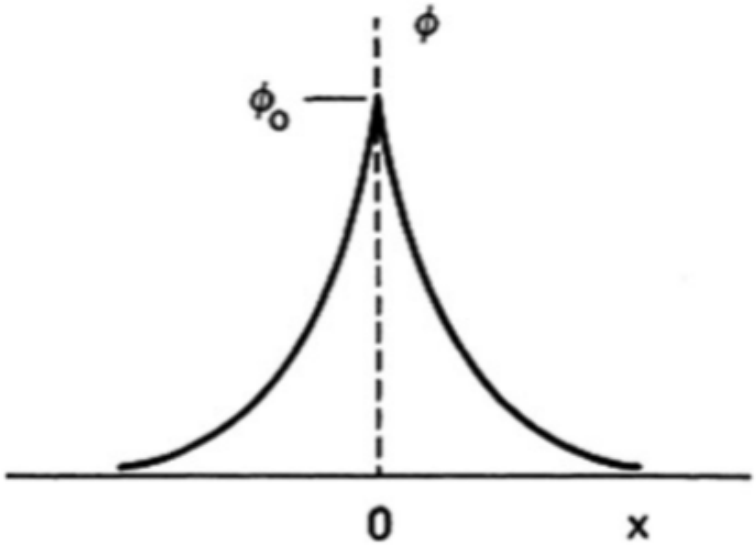

Figure 1.3: Potential distribution near a positively charged ball in a plasma. Adapted from [8]

If the system size L is much larger than the Debye length λ_D, then any electric field introduced to the plasma system will be shielded out in a tiny distance λ_D compared to L. Hence, the plasma system remains electrically neutral if it is neutral initially. If a

plasma is quasineutral, then one can take $n_i \simeq n_e$ (but not so neutral that all interesting electromagnetic forces vanish), and use the symbol n to denote the common density and call it the plasma density.

Plasma Oscillation

There are many kinds of oscillations in plasma, one of the most fundamental oscillations is the electron plasma oscillation. Imagine the ions are too heavy to move, and they form a uniform background. The electrons are then released from a distance away from the ions (Fig. 1.4). The electric field will pull the electrons toward the ions, after the electrons pass the ions, the electric field will decelerate them and started to pull them on the other side. The frequency of this oscillation is called plasma frequency,

$$\omega_p = \left(\frac{n_0 e^2}{\epsilon_0 m}\right)^{1/2} \tag{1.4}$$

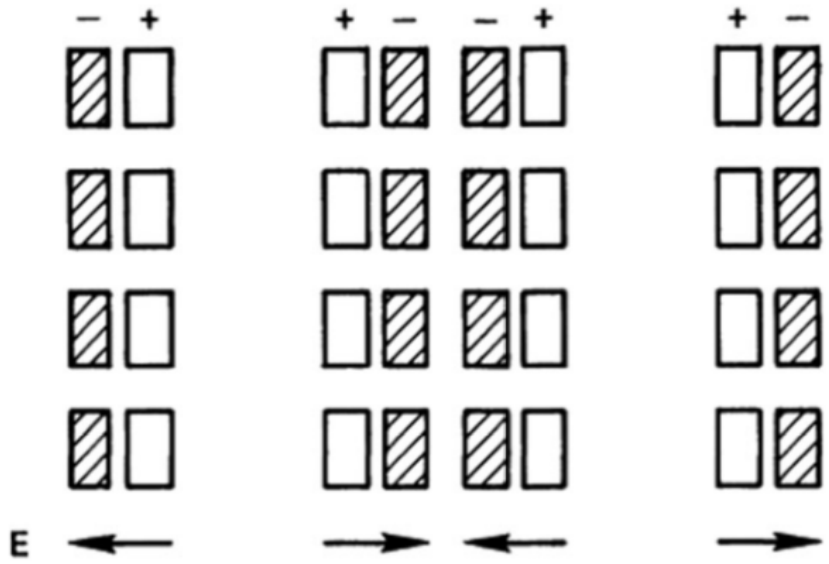

Figure 1.4: Mechanism of plasma oscillations. Adapted from [8].

Criteria of Plasmas

We are now able to give more detail definition for plasma. According to [8], not all ionized gas can be called plasma, there are three conditions a plasma must satisfy:

1. Debye length is much smaller than the system size, $\lambda_D \ll L$.
2. Collective behavior requires lots of particles in a Debye sphere, $N_D = n\frac{4\pi}{3}\lambda_D^3 \ggg 1$.

3. The gas behaves like plasma rather than a neutral gas, $\omega_p \tau > 1$ where ω_p typical plasma oscillation frequency and τ is the mean free time of collisions between neutral atoms.

1.2 Instability of Plasma Flow

The instability of plasma flow refers to the tendency of a plasma system to deviate from a stable, equilibrium state and exhibit perturbations or fluctuations in its behavior. It can be understood as the simple mechanical analogy with a ball on crest / in valley. On the left of Fig. 1.5 shows us a stable equilibrium, small perturbations given to the system will not push the ball far away from the equilibrium position, the valley. Hence, the equilibrium is stable. On the right, any small perturbations will cause the ball to fall downhill, hence the equilibrium is unstable. The instabilities in plasma can arise from various factors, such as the interaction of particles with electromagnetic fields, collective effects, or the presence of gradients in plasma parameters. A famous example of instability is the two stream instability. The configuration starts with two oppositely traveling beams of ions and electrons. As time evolves, chaotic behavior develops as shown in Fig. 1.6.

Figure 1.5: Mechanical analogy of various types of equilibrium. Adapted from [8]

Magnetic nozzle is one of the most actively researched configurations in plasma propulsion systems, which is being developed for space missions due to their potential for high efficiency and thrust. Understanding and controlling instabilities in the plasma flow within these nozzles is essential for optimizing their performance and achieving efficient propulsion. Investigating instabilities in plasma flow within magnetic nozzles also contributes to our broader understanding of fundamental plasma physics phenomena.

1.2.1 Analysis of Linear Instability

In this thesis, we will focus on the so-called linear instability. Meaning that the perturbation grows / decays only in exponential form. The following is a brief description of the process for analyzing linear instability. The detail treatment will be given in Chap. 2.

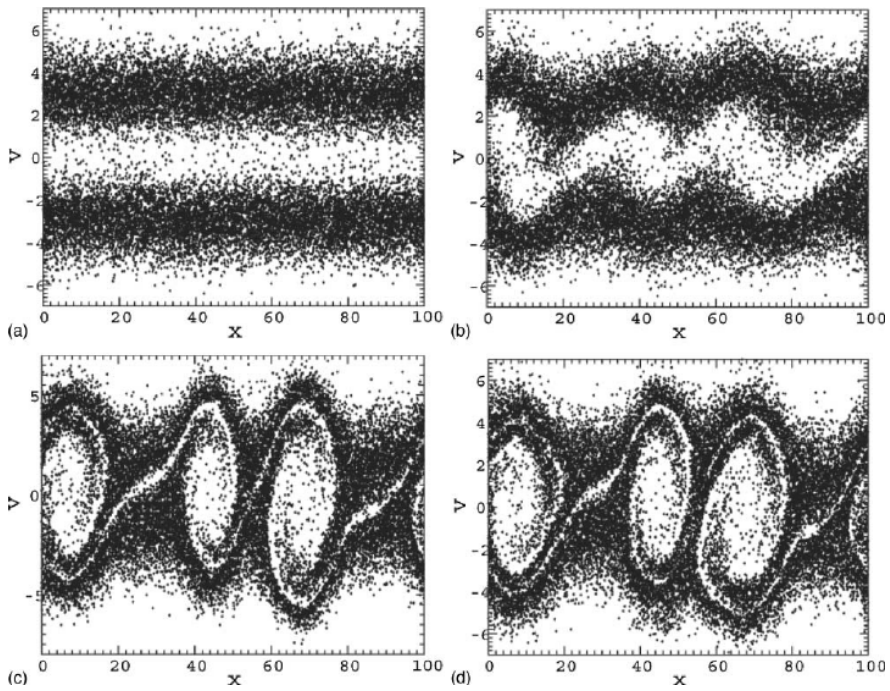

Figure 1.6: Visualization of two-stream instability in the phase space. (a) Initially the ion and electron flow are in opposite direction. (b) The velocity of both flows start to oscillate. (c) Chaotic behavior occurs. (d) The chaotic behavior continues. [15]

1. State equations of motion: The linear instability analysis starts from the equations of motion which describes the plasma system. In this thesis, the equations of motion are time-dependent fluid equations involving the number density n and velocity v of the plasma flow along the central axis of the nozzle.

2. Give perturbations to the system: Suppose the system has an equilibrium state n_0 and v_0. The system will be given small perturbations, they serve as small deviations on number density and velocity, $\tilde{n}$ and $\tilde{v}$. All variables n and v in the equations of motion will be substituted by perturbed quantities, $n_0 + \tilde{n}$ and $v_0 + \tilde{v}$.

3. Linearize equations of motion: Expand the equations of motion, and discard the second and higher order terms, often called nonlinear terms, such as $\tilde{n}\tilde{v}$, $\tilde{n}\partial_z\tilde{v}$, $\tilde{v}\partial_z\tilde{n}$ etc. We obtain the so-called linearized equations of motion. These equations contain only the linear terms.

4. Assume perturbation takes exponential form: Let perturbations take the form $\exp(-i\omega t)$. This indicates that the perturbations are oscillating with frequency ω in time. Any time derivative in the linearized equations of motion simply becomes $\partial_t = -i\omega$. Now we obtain equations involving perturbations, $\tilde{n}$ and $\tilde{v}$, and their spatial derivatives, and ω.

5. Analyze the possible values of ω: The oscillation frequency ω could be a complex number. If the imaginary part of the temporal frequency is greater than zero, i.e. $\mathrm{Im}(\omega) > 0$, then the system is unstable. This is because the perturbation grows exponentially $\exp(\mathrm{Im}(\omega)t)$ in time. On the other hand, if the imaginary part of the temporal frequency is less than or equal to zero, $\mathrm{Im}(\omega) \leq 0$, then the system is said to be stable. Since the perturbations will not be growing, $\mathrm{Im}(\omega) = 0$, or even damped, $\mathrm{Im}(\omega) < 0$.

In the later chapters, we devoted much effort to analyze the temporal frequency ω. We will employ spectral method to analyze the temporal frequency for subsonic and supersonic velocity profiles, and shooting method will be employed to obtain temporal frequency.

1.3 Magnetic Nozzle

In this thesis, we are going to deal with plasma flow in magnetic nozzle. A magnetic nozzle is a device that uses a magnetic field to shape and control the flow of charged particles in a plasma propulsion system, see Fig. 1.7. By employing magnetic mirrors, the magnetic nozzle can efficiently direct and accelerate the plasma particles, generating thrust for propulsion. The magnetic field in the nozzle helps collimate and focus the plasma exhaust, increasing its velocity and enhancing the performance of the propulsion system.

1.3.1 Magnetic Field in Magnetic Nozzle

The magnetic nozzle by its nature is 3-dimensional. We assume the magnetic field is axis-symmetric, then the radial magnetic field and axial magnetic field are constraint by divergence-free condition,

$$\boldsymbol{\nabla} \cdot \mathbf{B} = \frac{1}{r}\frac{\partial (rB_r)}{\partial r} + \frac{\partial B_z}{\partial z} = 0 \tag{1.5}$$

Since we are interested in the plasma flow near the central axis of the nozzle, paraxial approximation is taken. Meaning that we take the derivative along the magnetic field line $\nabla_{\parallel} = \partial/\partial z$ when near the central axis. Hence, in this thesis we will treat the flow in magnetic nozzle as a 1-dimensional problem. The axial magnetic field along the central axis is modeled as

$$B_z(z) = B_0 \left[1 + R\exp\left(-\left(\frac{z}{\delta}\right)^2\right)\right], \quad -1 \leq z \leq 1 \tag{1.6}$$

where $1 + R$ is the magnetic mirror ratio, it is the ratio of the magnitude of magnetic field at the center of the nozzle to that at the end of the nozzle, $1 + R = B(0)/B(1)$. The mirror ratio R controls the spread of the plasma flow at the exit. On the other hand, δ determines

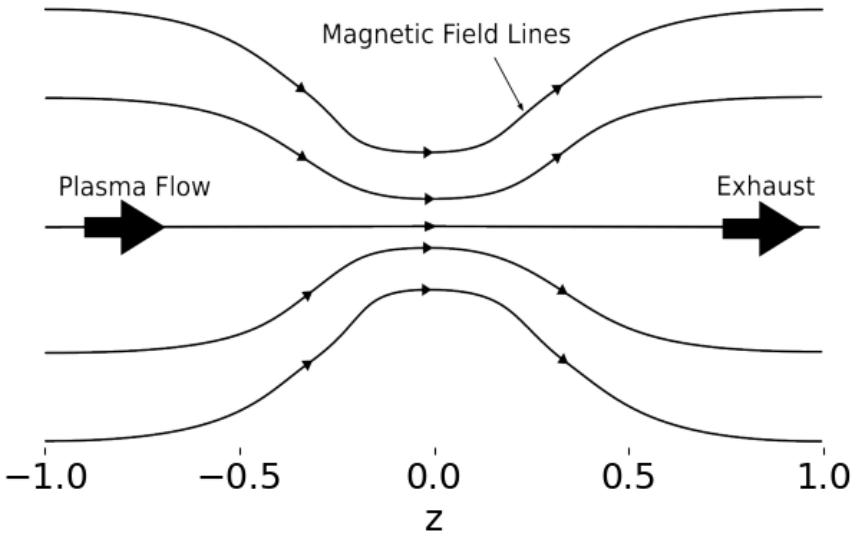

Figure 1.7: A simplified example of a magnetic nozzle configuration. On the left ($z = -1$) is the entrance of the nozzle. The plasma flows into the nozzle from the left and will be accelerated and finally exhaust through the exit on the right ($z = 1$). The magnetic field lines are shaped in such a way that it forms a magnetic mirror configuration. Plasma flow with specific subsonic speed at the entrance will be accelerated to supersonic speed.

the spread of the magnetic field. Larger the δ, flatter the magnetic field. An example of magnetic field is shown in Fig. (1.8).

The radial profile of magnetic field, B_r, is given by the divergence-free condition, Eq. (1.5). In this thesis will focus on the axial magnetic field only.

1.3.2 Velocity Profiles of Plasma Flow in Magnetic Nozzle

The analytical solution gives 4 different kinds of velocity profiles,

- Subsonic profile: Plasma flow enters and exits the nozzle with subsonic speed. Every point on this profile is subsonic.
- Supersonic profile: Plasma flow enters and exits the nozzle with supersonic speed. Every point on this profile is supersonic.
- Accelerating profile: Plasma flow enters the nozzle with subsonic speed and exits the nozzle with supersonic speed. Points before the nozzle throat are subsonic, and the flow reaches ion sound speed at the nozzle throat, then the flow is supersonic after the nozzle throat.
- Decelerating profile: Plasma flow enters the nozzle with supersonic speed and exits

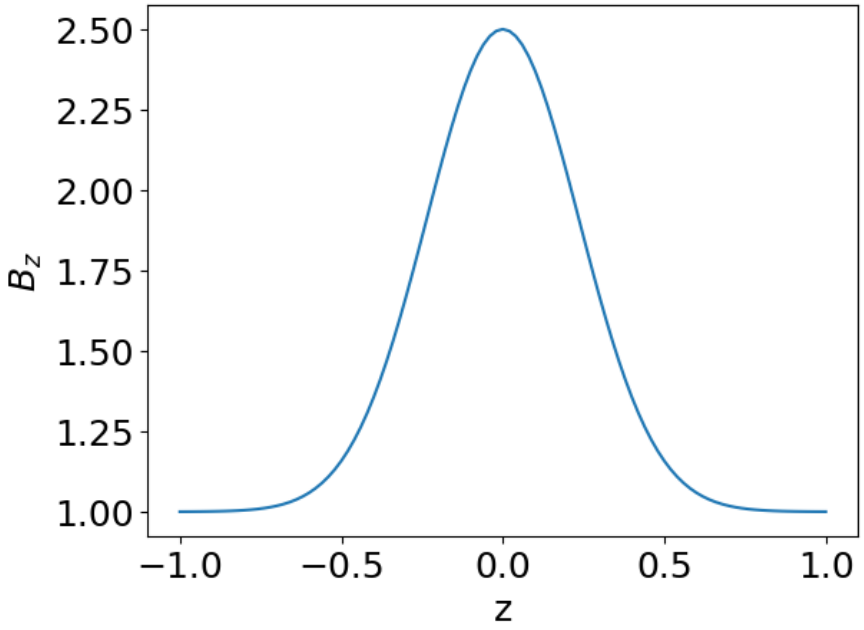

Figure 1.8: This is the magnetic field in nozzle with mirror ratio $1 + R = B_{max}/B_{min} = 2.5$, and the spread of magnetic field, $\delta = 0.1/0.3 = 0.\bar{3}$.

the nozzle with subsonic speed. Similar to the accelerating profile, but the velocity is decreasing.

See Fig. 2.3 for these profiles.

The velocity of plasma flow in the magnetic nozzle is given by the Lambert W function, Eq. (2.14). The Lambert W function has 2 different branches. The $k = 0$ branch corresponds to the subsonic parts in the velocity profile, and the $k = -1$ branch gives the supersonic parts. The expression of velocity profile will be derived in Chap. 2 and more details will be discussed.

1.4 Flow in Similar Configuration: Bondi-Parker Flow

Consider a massive celestial object in the space. This celestial object will attract matter in the space because it is massive. Hence, creating an accretion flow. If the celestial object is a star, it can also eject matter into space. Solar wind is an example to this since it is a stream of charged particles, primarily electrons and protons, flowing outward from the Sun. Bondi derived a steady-state solution for accretion flow which is governed by Bernoulli's equation in spherical symmetry around a point mass in 1952. Hence, the inward accretion flow is also called Bondi flow. Then Parker solved a similar problem but with outward wind in 1958. Then the outward wind is given the name, Parker flow. [2, 4, 18] The Bondi and Parker flow (also called Bondi-Parker flow) is similar to that in magnetic nozzle. It is interesting to

compare the two configurations.

If we compare the velocity profiles for Bondi-Parker flow and the flow in magnetic nozzle. We found they are similar. The Bondi-Parker flow can also be grouped into the following types: subsonic, supersonic, and transonic (accelerating and decelerating). See Fig. 1.9. For subsonic profiles, every point on the curve is slower than sound speed. While every point on the supersonic velocity profile is faster than sound speed. Lastly, there are two different transonic profiles: accelerating profile and decelerating profile. The accelerating profile describes the accelerating plasma flow which is at subsonic speed at the mass point, e.g. a star, and is accelerated to supersonic speed far away. The decelerating profile shows that a plasma flow ejected supersonically from a mass point and then decelerated to subsonic speed far away.

The velocity profiles of one-dimensional, spherically symmetric, stationary isothermal Parker flow neglecting self-gravity can be expressed using Lambert W function,

$$v(r) = \sqrt{-\frac{KT}{m} W_k \left[-\left(\frac{r}{r_c}\right)^2 \exp\left[4\left(1-\frac{r_c}{r}\right)-1\right]\right]}, \quad k = 0, -1 \tag{1.7}$$

where r stands for the distance measured from the center of the mass point, e.g. star. The position $r_c = GMm/2KT$ is the critical position and the velocity at this point is exactly the sonic speed $v(r_c) = \sqrt{KT/m}$, where M is the mass of the mass point, m is the mass of a single particle in the flow, and T is the temperature of the flow. The Bondi flow is simply $-v(r)$ since it is accretion flow, the particles are flowing inwardly towards the mass point.

As we can see the expression of velocity profile for Bondi-Parker flow is similar to that of the magnetic nozzle, Eq. (2.14). The expression is governed by the Lambert W function. Similarly, the $k = 0$ branch corresponds to the subsonic part in the velocity profile, and the $k = -1$ branch corresponds to the supersonic part of the profile.

The instabilities of the Bondi-Parker flow has been extensively studied. [**?**, 35, 36, 11, 18] Hopefully these studies can provide insights into our problem.

1.5 Goals of this Thesis

Fusion is considered the next-generation source of a clean, safe and abundant energy providing an opportunity to address climate change problems. A new high-tech industry has appeared in the last decade fueled by over $4 billion of private investments, with the second world largest and several other smaller companies founded in Canada. To achieve controlled fusion, one of the key science problems is to understand and learn to predict the non-linear behavior

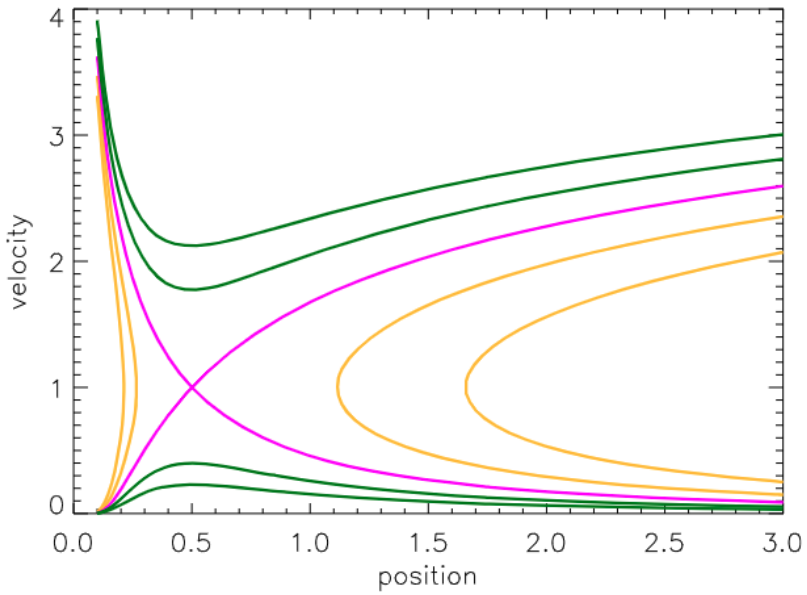

Figure 1.9: Representative trajectories of the steady-state BP flow in non-dimensional units. The velocities are shown in absolute values. Adapted from [18]. The upward pink line represents an accelerating flow, it accelerates from subsonic to supersonic. The downward pink line represents a decelerating flow. The green lines below the pink lines represent subsonic flows, and the green lines above represent supersonic flows. Orange lines are physically impossible scenarios. If the sign of the velocity is positive, then it is an outward (Parker) flow, otherwise it is an inward (Bondi) flow.

of plasma due to waves and instabilities. The general objective of my research is to understand the behavior and learn to control the turbulent flows of plasmas in magnetically controlled fusion system, in particular, open magnetic mirrors. I study the instabilities of the flow in a magnetic mirror configuration under different boundary conditions which is an open question and is under debate in application to fusion systems and also related to the solar wind flows.

The general objective of this research is to understand the stability of the flow in a magnetic nozzle. Plasma confined by the magnetic field is typically far from the state of the thermodynamic equilibrium which makes it unstable. In this project, we would like to investigate the stability of plasma flow in a magnetic nozzle under different boundary conditions. Understanding the instabilities of plasma flow in a magnetic mirror configuration is important in applications such as the expanding magnetic divertors in controlled fusion and electric propulsion. [28, 17]

In the following thesis, fluid model of plasma will be reviewed and linearized governing equations will be derived in chapter 2. The problem will be then formulated as an eigenvalue problem. In chapter 3, spectral method and shooting method for solving eigenvalue problem will be introduced. In the section of spectral method, different discretizations of the operators, such as finite difference and spectral method will be discussed. Moreover, spectral pollution and its filtering will as also be investigated. Then in the next section, we will formulate the problem to the form suitable for applying shooting method. We will apply both shooting method and spectral method to the problem. By comparing the results from two different methods, the credibility of the results are increased. In chapter 5, we will use the method developed in chapter 3 to conduct numerical experiments. The goal is to extract the eigenvalues (frequency) of each oscillating mode. Conclusion will in chapter 6.

Chapter 2

Theoretical Analysis

In this chapter, we start from the fluid description of plasma, and derive the governing equations for the flow in magnetic nozzle. After this, we linearize the governing equations and reformulate the problem as a polynomial eigenvalue problem. Then a special case is discussed analytically.

2.1 Kinetic Theory

2.1.1 Single Particle Motion Along Magnetic Field Line

Plasma consists of charged particles, and is governed by electromagnetic force. Assume magnetic field only, the particle motion is governed by Lorentz force and the particles will gyrate along the magnetic field lines. The equation of motion of a charged particle in magnetic field is given by

$$m\frac{\mathrm{d}\mathbf{v}_p}{\mathrm{d}t} = q\mathbf{v}_p \times \mathbf{B}$$

where m is the mass of charged particle, q is the charge of particles, and $\mathbf{v}_p$ is the velocity of the particle.

Consider a magnetic field pointing in z-direction, $\mathbf{B} = B\hat{\mathbf{z}}$. Since the magnetic force is perpendicular to both $\mathbf{v}_p$ and $\mathbf{B}$, we can separate the equation of motion into two directions,

$$q\mathbf{v}_\perp \times \mathbf{B} = \frac{mv_\perp^2}{r}\hat{\mathbf{r}}, \quad \mathbf{v}_\parallel = v_\parallel\hat{\mathbf{z}}$$

where $\mathbf{v}_\perp$ is the velocity perpendicular to the magnetic field, and $\mathbf{v}_\parallel$ is the velocity parallel to the magnetic field, and $\hat{\mathbf{r}}$ is a unit vector pointing from the central axis of the helical motion to the trajectory of the particle. In this way, we see that the charged particle is doing circular motion in the plane of $\hat{\mathbf{r}}$, gyrating along the magnetic field line with Larmor radius r

and Larmor frequency $\omega_c = |q|B/m$. On the other hand, the particle is flowing freely in the direction of **B** since there is no force in this direction. The charged particle is doing helical motion along the magnetic field line.

2.1.2 Adiabatic Invariants

The charged particles always travel on the same magnetic field line in the magnetic nozzle. To show this we will introduce two adiabatic invariants.

Magnetic Moment

In classical mechanics, the action integral $\oint pdq$ taken over a period of a periodic motion is a constant. Here p and q are generalized momentum and coordinate. In single particle motion along magnetic field line, one obvious periodic motion is the Larmor gyration. Take p to be the angular momentum $mv_\perp r$ and q to be the angular coordinate θ, the action integral becomes

$$\oint pdq = \oint mv_\perp r_L d\theta = 2\pi r_L m v_\perp = 2\pi \frac{mv_\perp^2}{\omega_c} = 4\pi \frac{m}{|q|}\left(\frac{mv_\perp^2}{2B}\right) \tag{2.1}$$

Define the quantity magnetic moment as

$$\mu = \frac{mv_\perp^2}{2B} \tag{2.2}$$

We see that the magnetic moment μ is constant as long as q/m is constant.

Longitudinal Invariant

The next adiabatic invariant is the quantity defined as [8]

$$J = \int_a^b v_\parallel ds \tag{2.3}$$

where a and b are the two turning points in magnetic mirror, see Fig. 2.1.

Since the particle's energy is conserved and is equal to $mv_\perp^2/2$ at the turning point, the invariance of μ indicates that $|B|$ remains the same at the turning point. However, upon drifting back to the same longitude, a particle may find itself on another line of force at a different altitude. This cannot happen if J is conserved. J determines the length of the line of force between turning points, and no two lines have the same length between points with the same $|B|$. Consequently, the particle returns to the same line of force even in a slightly asymmetric field.

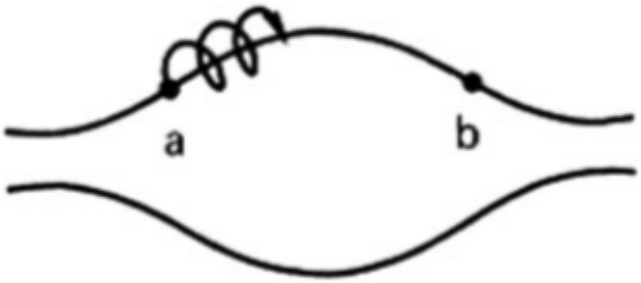

Figure 2.1: A particle bouncing between turning points a and b in a magnetic field. Adapted from [8].

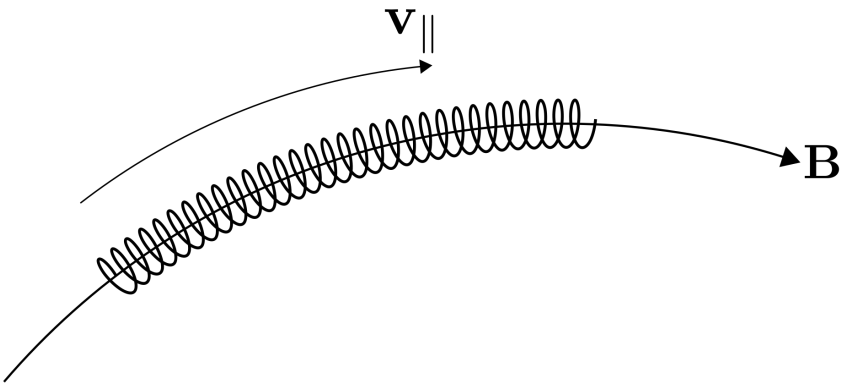

Figure 2.2: A charged particle gyrates about the magnetic field line. The velocity along the field line is $\mathbf{v}_{\|}$ and the gyrate frequency, radius is given by the radial equation, $q\mathbf{v}_{\perp} \times \mathbf{B} = \hat{\mathbf{r}} m v_{\perp}^2 / r$. Moreover, for static, nonuniform magnetic field, the charged particle will stay on the same of magnetic field line as it gyrates.

2.1.3 From Kinetic Theory to Fluid Description

Although the previous treatment is useful for single particle, to describe the collective behavior of a large amount of particles, we need to do that in the framework of kinetic theory. In kinetic theory, the charged particles in plasma obey a certain distribution function,

$$f(\mathbf{x}, \mathbf{v}_p, t)$$

It describes the probability density at position $\mathbf{x}$ with velocity $\mathbf{v}$ at time t.

Suppose a collisionless plasma in 3-dimensional space is at thermal equilibrium, then the particles can be characterized by Maxwell-Boltzmann distribution

$$f_M(\mathbf{x}, \mathbf{v}_p, t) = \frac{n(\mathbf{x}, t)}{(\pi v_{th}^2)^{3/2}} \exp\left(-\left(\frac{v}{v_{th}}\right)^2\right)$$

where $n(\mathbf{x}, t)$ is number density of the particles, $v_{th} = \sqrt{2k_B T/m}$ is the thermal velocity, and $v = \sqrt{v_x^2 + v_y^2 + v_z^2}$.

The moments of the distribution function are suitable macroscopic properties of the plasma. For example, the plasma number density and momentum can be viewed as

$$n(\mathbf{x}, t) = \int_{\mathbb{R}^3} f(\mathbf{x}, \mathbf{v}_p, t) d^3\mathbf{v}_p$$

$$n\mathbf{v}(\mathbf{x}, t) = \int_{\mathbb{R}^3} \mathbf{v}_p f(\mathbf{x}, \mathbf{v}_p, t) d^3\mathbf{v}_p$$

where $\mathbf{v}$ is the fluid velocity of the charged particle. It is the bulk velocity of the plasma. The charged particles flow along the magnetic field line, it is intuitive to think of $\mathbf{v}$ as the plasma flow velocity along the magnetic field line.

In this thesis we assume collisionless plasma. The distribution function f in a collisionless plasma satisfies the so-called collisionless Vlasov equation, $\mathrm{d}/\mathrm{d}t\, f(\mathbf{x}, \mathbf{v}, t) = 0$. Expand it explicitly, it is

$$\frac{\partial f}{\partial t} + \mathbf{v}\frac{\partial f}{\partial \mathbf{x}} + \frac{q}{m}(\mathbf{E} + \mathbf{v} \times \mathbf{B})\frac{\partial f}{\partial \mathbf{v}} = 0 \tag{2.4}$$

where $q(\mathbf{E} + \mathbf{v} \times \mathbf{B})$ is the Lorentz force experience by the species, the collision term $C(f)$ is dropped.

Integrate both sides with respect to volume element in velocity space, $d^3\mathbf{v}$, we get the conservation of density.

$$\frac{\partial n}{\partial t} + \boldsymbol{\nabla} \cdot (n\mathbf{v}) = 0 \tag{2.5}$$

If we multiply $\mathbf{v}$ on both sides and integrate with respect to $d^3\mathbf{v}$, we get the conservation

of momentum.

$$n\frac{\partial \mathbf{v}}{\partial t} + \mathbf{v} \cdot \boldsymbol{\nabla}\mathbf{v} = \frac{q}{m}(\mathbf{E} + \mathbf{v} \times \mathbf{B}) - \boldsymbol{\nabla} p \tag{2.6}$$

In the process we assume isotropic pressure, and no viscosity exists in the plasma.

As we can see the fluid description only depends on the macroscopic properties of plasma, such as the fluid velocity along the magnetic field line $\mathbf{v}$, number density n, and pressure p of the plasma. This simplifies the problem.

2.2 Fluid Description for Flow

In this section, we will derive the governing equations of the flow in magnetic nozzle, starting from the fluid description for plasma.

We start by deriving the usefule form of the conservation of density,

$$\frac{\partial n}{\partial t} + \boldsymbol{\nabla} \cdot (n\mathbf{v}) = 0$$

where $\mathbf{v}$ here denotes the fluid velocity of the plasma flow.

We can get the fluid velocity by taking the integral

$$\mathbf{v} = \frac{1}{n}\int_{\mathbb{R}^3} \mathbf{v}_p f(\mathbf{x}, \mathbf{v}_p, t) d^3\mathbf{v}_p$$

Denote the particle velcity as $\mathbf{v}_p$, we can decompose the particle velocity vector as $\mathbf{v}_p = (v_\parallel, v_\perp)$, where $v_\parallel$ and $v_\perp$ are the magnitudes of components that are parallel to and perpendicular to the magnetic field line, respectively. Due to the Lorentz force, the charged particles gyrates about the magnetic field lines, see Fig. 2.2. Hence, the $v_\perp$ will be averaged to zero the expression for plasma fluid velocity can be simplied as

$$\mathbf{v} = v\mathbf{B}/B$$

where v is the fluid speed along the magnetic field lines. This makes sence because the charged particles flows along $\mathbf{B}$.

By expanding the divergence term, and using the divergence free condition $\boldsymbol{\nabla} \cdot B = 0$, we have

$$\frac{\partial n}{\partial t} + \mathbf{B} \cdot \boldsymbol{\nabla}\Big(\frac{nv}{B}\Big) = 0$$

Since the magnetic field lines are aligned with the central axis of the nozzle, which we denote

as z-axis, so $\mathbf{B} = B\hat{z}$. Now we obtain the conservation of density for the magnetic nozzle,

$$\frac{\partial n}{\partial t} + B\frac{\partial}{\partial z}\Big(\frac{nv}{B}\Big) = 0 \tag{2.7}$$

The second governing equation is the conservation of momentum,

$$mn\frac{\partial \mathbf{v}}{\partial t} + mn\mathbf{v}\cdot\boldsymbol{\nabla}\mathbf{v} = -\boldsymbol{\nabla}p$$

where m is the ion mass. This equation tells us the plasma flow is driven by pressure.

The equation of state is given by the isothermal condition,

$$p = nk_BT \tag{2.8}$$

There are two main reasons. First the plasma particles are confined to the magnetic field lines. This reduces the particle collisions and energy exchanges. Moreover, the electrons have high mobility, they will quickly fill up any charge cavities and thus maintain a constant temperature. Hence, we can safely assume the plasma flow is isothermal.

Therefore, we have

$$\frac{\partial v}{\partial t} + v\frac{\partial v}{\partial z} = -c_s^2\frac{1}{n}\frac{\partial n}{\partial z} \tag{2.9}$$

where $c_s^2 = k_BT/m$ is the square of sound speed.

Therefore, the dynamics of the plasma flow in magnetic nozzle can be characterized by the conservation of density and momentum,

$$\frac{\partial n}{\partial t} + B\frac{\partial}{\partial z}\Big(\frac{nv}{B}\Big) = 0$$
$$\frac{\partial v}{\partial t} + v\frac{\partial v}{\partial z} = -c_s^2\frac{1}{n}\frac{\partial n}{\partial z}$$

The magnetic field profile was discussed in Sec.1.3.1.

In this research, we are interested in the stability of the equilibrium flow in the nozzle. Let's denote n_0 and v_0 as equilibrium density and equilibrium velocity, respectively. Since they are stationary (time independent) solutions to the above set of equations, so they satisfy the so-called equilibrium condition,

$$B\frac{\partial}{\partial z}\Big(\frac{n_0v_0}{B}\Big) = 0$$
$$v_0\frac{\partial v_0}{\partial z} = -c_s^2\frac{1}{n_0}\frac{\partial n_0}{\partial z}$$

2.3 Non-dimensionalization

For convenience, we nondimensionalize the governing equations by normalizing the velocity to c_s, $v \mapsto v/c_s$, z to system length L, $z \mapsto z/L$ and time $t \mapsto c_s t/L$. The governing equations become

$$\frac{\partial n}{\partial t} + n\frac{\partial v}{\partial z} + v\frac{\partial n}{\partial z} - nv\frac{\partial_z B}{B} = 0 \tag{2.10}$$

$$n\frac{\partial v}{\partial t} + nv\frac{\partial v}{\partial z} = -\frac{\partial n}{\partial z} \tag{2.11}$$

and the nondimensionalized equilibrium condition is

$$\frac{\partial}{\partial z}\Big(\frac{n_0 v_0}{B}\Big) = 0 \tag{2.12}$$

$$v_0\frac{\partial v_0}{\partial z} = -\frac{1}{n_0}\frac{\partial n_0}{\partial z} \tag{2.13}$$

2.4 Velocity Profiles at Equilibrium

In this section we will solve the equilibrium velocity profile, v_0, from the nondimensionalized equilibrium condition, Eq. (2.12) and Eq. (2.13). We start by substituting $\frac{1}{n_0}\,\partial n_0/\partial z$ into Eq. (2.12), then it becomes

$$(v_0^2 - 1)\frac{\partial v_0}{\partial z} = -\frac{v_0}{B}\frac{\partial B}{\partial z}$$

Notice that there is a singularity at $v_0 = 1$, the sonic speed.

This is a separable equation, integrate it and use the conditions at midpoint $B(0) = B_m, v_0(0) = v_m$ we get

$$v_0^2 e^{-v_0^2} = \frac{B^2}{B_m^2} v_m^2 e^{-v_m^2}$$

We can now express v_0 using the Lambert W function (see Appendix A),

$$v_0(z) = \left[-W_k\left(-\frac{B(z)^2}{B_m^2} v_m^2 e^{-v_m^2}\right)\right]^{1/2} \tag{2.14}$$

where the subscript k of W stands for branch of Lambert W function.

When considering the velocity profile of a nozzle flow, various scenarios can be distinguished based on the Mach number parameter (v_m) and the branch (k) used in the expression for the Mach number distribution, denoted as $v_0(z)$. These parameters play a crucial role in determining the flow characteristics. The selection of appropriate v_m and k values facilitates the control of the flow characteristics in the nozzle, allowing for the realization of various

flow regimes, such as subsonic, supersonic, transonic, accelerating, or decelerating profiles. Different velocity profiles are shown in Fig. 2.3.

Firstly, for the case where $v_m < 1$ and $k = 0$, the resulting velocity profile is classified as subsonic. This means that both at the entrance and exit of the nozzle, the velocity remains subsonic, and the midpoint velocity is also less than unity ($v_m < 1$). A subsonic flow is characterized by fluid velocities that are slower than the local speed of sound.

On the other hand, when $v_m > 1$ and $k = -1$, the velocity profile corresponds to a supersonic flow regime. In this situation, the fluid velocities at both the entrance and exit of the nozzle are supersonic, and the midpoint velocity (v_m) exceeds the value of unity ($v_m > 1$). Supersonic flow is characterized by velocities that surpass the speed of sound.

Furthermore, when $v_m = 1$, the velocity profile becomes transonic. In this case, the midpoint velocity is exactly at the sonic threshold ($v_m = 1$), where the fluid velocity equals the local speed of sound. Transonic flows often exhibit a combination of subsonic and supersonic regions, and this regime poses unique challenges due to the presence of singularity at the nozzle throat. We will discuss this thoroughly in Chap. 4.

To achieve an accelerating velocity profile, a configuration with $k = 0$ for $x < 0$ and $k = -1$ for $x > 0$ is employed. Here, x represents the spatial coordinate along the nozzle length. With this setup, the flow starts subsonically and gradually accelerates to a supersonic speed as it propagates along the nozzle.

Conversely, a decelerating velocity profile can be obtained by adopting a similar approach but with reversed values of k. Specifically, the configuration will have $k = -1$ for $x < 0$ and $k = 0$ for $x > 0$, causing the flow to start supersonically and decelerate to subsonic velocities further down the nozzle.

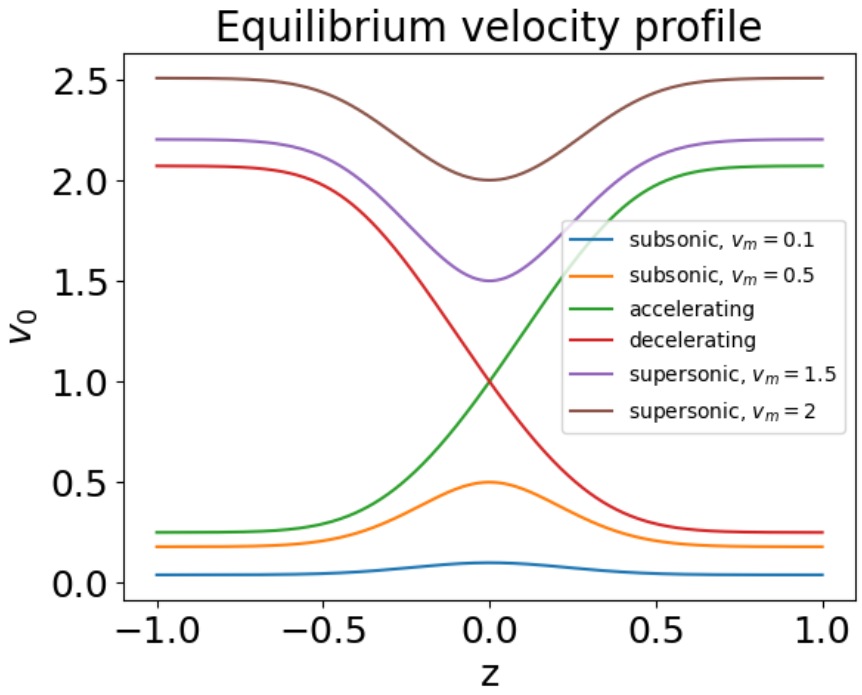

Figure 2.3: The velocity profile in the magnetic nozzle is completely determined by the midpoint mach number v_m and the branch k. A subsonic profile can be obtained by selecting $v_m < 1$ and $k = 0$. On the other hand, a supersonic profile can be obtained by setting $v_m > 1$ and $k = -1$. Lastly, for the transonic velocity profiles, the midpoint velocity is set to unity, $v_m = 1$, and then by choose $k = 0$ for $x < 0$ and $k = -1$ for $x > 0$ we get accelerating profile. Decelerating profile can be obtained similarly.

2.5 Linearized Governing Equations

As illustrated in Sec.??, it is essential to linearize the governing equations in order to investigate the instability of plasma. Now we are going to derive the linearized governing equations with the equilibrium conditions given in above.

Let $n = n_0(z) + \tilde{n}(z,t)$ and $v = v_0(z) + \tilde{v}(z,t)$, where $\tilde{n}$ and $\tilde{v}$ are small perturbed quantities.

We first linearize Eq. (2.10) by setting $n = n_0 + \tilde{n}$ and $v = v_0 + \tilde{v}$,

$$\frac{\partial(n_0+\tilde{n})}{\partial t} + (n_0+\tilde{n})\frac{\partial(v_0+\tilde{v})}{\partial z} + (v_0+\tilde{v})\frac{\partial(n_0+\tilde{n})}{\partial z} - (n_0+\tilde{n})(v_0+\tilde{v})\frac{\partial_z B}{B} = 0$$

By ignoring the second order perturbations, we obtain

$$\frac{1}{n_0}\frac{\partial\tilde{n}}{\partial t} + \frac{\partial v_0}{\partial z} + \frac{\tilde{n}}{n_0}\frac{\partial v_0}{\partial z} + \frac{\partial\tilde{v}}{\partial z} + \frac{v_0}{n_0}\frac{\partial n_0}{\partial z} + \frac{\tilde{v}}{n_0}\frac{\partial n_0}{\partial z} + \frac{v_0}{n_0}\frac{\partial\tilde{n}}{\partial z} - v_0\frac{\partial_z B}{B} - \tilde{v}\frac{\partial_z B}{B} - \tilde{n}\frac{v_0}{n_0}\frac{\partial_z B}{B} = 0$$

Using the equilibrium condition Eq. (2.12), some of the terms are canceled. Moreover, the last term can be written as

$$\tilde{n}\frac{v_0}{n_0}\frac{\partial_z B}{B} = \frac{\tilde{n}}{n_0}\left(\frac{\partial_z n_0}{n_0}v_0 + \frac{\partial v_0}{\partial z}\right)$$

Now, we get the linearized conservation of mass,

$$\frac{1}{n_0}\frac{\partial \tilde{n}}{\partial t} + \frac{\partial \tilde{v}}{\partial z} + v_0\tilde{Y} + \tilde{v}\frac{\partial_z n_0}{n_0} - \tilde{v}\frac{\partial_z B}{B} = 0 \tag{2.15}$$

where

$$\tilde{Y} \equiv \frac{1}{n_0}\frac{\partial \tilde{n}}{\partial z} - \frac{\partial_z n_0}{n_0^2}\tilde{n} = \frac{\partial}{\partial z}\left(\frac{\tilde{n}}{n_0}\right)$$

To linearize the conservation of momentum, we follow the same logic by substituting $n = n_0 + \tilde{n}$, and $v = v_0 + \tilde{v}$ in Eq. (2.11),

$$(n_0 + \tilde{n})\frac{\partial(v_0 + \tilde{v})}{\partial t} + (n_0 + \tilde{n})(v_0 + \tilde{v})\frac{\partial(v_0 + \tilde{v})}{\partial z} = -\frac{\partial n}{\partial z}$$

Again, ignore second order perturbations and rearange terms, we have

$$\frac{\partial v_0}{\partial t} + v_0\frac{\partial v_0}{\partial z} + \tilde{v}\frac{\partial v_0}{\partial z} = -\frac{1}{n_0}\frac{\partial n_0}{\partial z} - \frac{1}{n_0}\frac{\partial \tilde{n}}{\partial z} - v_0\frac{v_0}{z} - \frac{\tilde{n}}{n_0}v_0\frac{\partial v_0}{\partial z}$$

Using the equilibrium condition Eq. (2.13) on the RHS, we get the linearized conservation of momentum,

$$\frac{\partial \tilde{v}}{\partial t} + \frac{\partial(v_0\tilde{v})}{\partial z} = -\tilde{Y} \tag{2.16}$$

2.6 Polynomial Eigenvalue Problem

We can further simplify the problem by combining Eq. (2.15) and Eq. (2.16) into a single equation. We can substitute Eq. (2.16) into Eq. (2.15) to eliminate $\tilde{Y}$,

$$\frac{\partial}{\partial t}\frac{\tilde{n}}{n_0} + \frac{\partial \tilde{v}}{\partial z} - v_0\left(\frac{\partial}{\partial t}\tilde{v} + \frac{\partial(v_0\tilde{v})}{\partial z}\right) + \tilde{v}\frac{\partial_z n_0}{n_0} - \tilde{v}\frac{\partial_z B}{B} = 0 \tag{2.17}$$

In order to investigate the instability of the flow, we need formulate it as an eigenvalue problem. To do that, we assume the perturbed density and velocity are oscillatory, i.e. $\tilde{n}, \tilde{v} \sim \exp(-i\omega t)$, where ω is the oscillation frequency of the perturbed quantities. This frequency can be a complex number.

As illustrated in Sec.**??**, the flow can be stable or unstable depending on the imaginary

part of the frequency. If $\mathrm{Im}(\omega) > 0$, then the perturbed quantities $\tilde{n} \sim \exp(\mathrm{Im}(\omega)t)$, which means it grows exponentially with time, hence unstable. If $\mathrm{Im}(\omega) \leq 0$, then the amplitude of the perturbed quanties are either unchanged or exponentially decreasing, hence the flow is stable.

By assuming oscillatory perturbed quantities, Eq. (2.17) becomes,

$$-i\omega\frac{\tilde{n}}{n_0} + \frac{\partial\tilde{v}}{\partial z} - v_0\left(-i\omega\tilde{v} + \frac{\partial(v_0\tilde{v})}{\partial z}\right) + \tilde{v}\frac{\partial_z n_0}{n_0} - \tilde{v}\frac{\partial_z B}{B} = 0 \tag{2.18}$$

Using the equilibrium condition Eq. (2.12), we can eliminate the term $\partial_z B/B$,

$$-i\omega\frac{\tilde{n}}{n_0} + \frac{\partial\tilde{v}}{\partial z} + v_0\left(i\omega\tilde{v} - v_0\frac{\partial\tilde{v}}{\partial z} - \tilde{v}\frac{\partial v_0}{\partial z}\right) - \tilde{v}\frac{\partial_z v_0}{v_0} = 0$$

Rearrange terms, we have

$$-i\omega\frac{\tilde{n}}{n_0} + i\omega v_0\tilde{v} + (1 - v_0^2)\frac{\partial\tilde{v}}{\partial z} - \left(v_0 + \frac{1}{v_0}\right)\frac{\partial v_0}{\partial z}\tilde{v} = 0$$

Now we take $\partial/\partial t$ on Eq. (2.16). Recall the fact that $\tilde{Y} = \partial_z(\tilde{n}/n_0)$, we have

$$\omega^2\tilde{v} + i\omega\left(v_0\frac{\partial\tilde{v}}{\partial z} + \tilde{v}\frac{\partial v_0}{\partial z}\right) = \frac{\partial}{\partial t}\frac{\partial}{\partial z}\left(\frac{\tilde{n}}{n_0}\right)$$

Apply ∂_t operator first, we get

$$\omega^2\tilde{v} + i\omega\left(v_0\frac{\partial\tilde{v}}{\partial z} + \tilde{v}\frac{\partial v_0}{\partial fz}\right) = \frac{\partial}{\partial z}\left(-i\omega v_0\tilde{v} - (1 - v_0^2)\frac{\partial\tilde{v}}{\partial z} + \left(v_0 + \frac{1}{v_0}\right)\frac{\partial v_0}{\partial z}\tilde{v}\right)$$

Expand the RHS and collect terms, we get

$$\begin{aligned}
&\omega^2\tilde{v} \\
&+ 2i\omega\left(v_0\frac{\partial}{\partial z} + \frac{\partial v_0}{\partial z}\right)\tilde{v} \\
&+ \left[(1 - v_0^2)\frac{\partial^2}{\partial z^2} - \left(3v_0 + \frac{1}{v_0}\right)\frac{\partial v_0}{\partial z}\frac{\partial}{\partial z} - \left(1 - \frac{1}{v_0^2}\right)\left(\frac{\partial v_0}{\partial z}\right)^2 - \left(v_0 + \frac{1}{v_0}\right)\frac{\partial^2 v_0}{\partial z^2}\right]\tilde{v} = 0
\end{aligned} \tag{2.19}$$

In mathematical terms, Eq. (2.19) is a polynomial eigenvalue problem, where ω is an eigenvalue to the problem, and the velocity perturbation $\tilde{v}$ is an eigenfunction associated with the eigenvalue ω. In the later chapters we will discuss the methods to tackle this problem.

2.7 Analytical Solutions to Constant Velocity Case

In this section we are going to tackle the simplest case of the polynomial eigenvalue problem, Eq. (2.19), the constant velocity case.

The constant velocity profile can be viewed as the limit of $v_0(z)$ as the spread of magnetic field goes to infinity, $\delta \to \infty$. As the parameter δ approaches infinity, the width of the magnetic field enlarges and eventually becomes flat. In other words, a constant magnetic field. We can easily see that the velocity profile $v_0(z)$ becomes a constant as well.

If we set the velocity profile of the equilibrium flow to constant $v_0 = \text{const}$, then Eq. (2.19) becomes a simple boundary value problem with second order constant coefficients differential equation.

$$\omega^2 \tilde{v} + 2i\omega v_0 \frac{\partial \tilde{v}}{\partial z} + (1 - v_0^2) \frac{\partial^2 \tilde{v}}{\partial z^2} = 0 \tag{2.20}$$

We need two boundary values in order to uniquely determine the solution (up to a constant). In the following subsections, we will solve Eq. (2.19) with constant velocity under two sets of boundary conditions, Dirichlet and fixed-open boundary condition.

2.7.1 Dirichlet Boundary

In this subsection, the so-called Dirichlet boundary condition will be used. It has the name because the function values are fixed at the two ends of the nozzle,

$$\tilde{v}(-1) = \tilde{v}(1) = 0$$

At the left end (entrance of the nozzle), $z = -1$, we assume there are no perturbations. As for the right end (exit of the nozzle), $z = 1$, setting the velocity perturbation to 0 might not be the best boundary condition to describe the physical process of the plasma flow in the nozzle, it nevertheless serves as a starting point to the problem.

With the two boundary conditions, we are able to determine the solution to this problem,

$$\tilde{v}(z) = C \left[\exp\left(i\omega \frac{z+1}{v_0+1} \right) - \exp\left(i\omega \frac{z+1}{v_0-1} \right) \right] \tag{2.21}$$

where $C \in \mathbb{C}$ is a complex constant, and the frequencies are $\omega = n\pi(1 - v_0^2)/2$ with $n \in \mathbb{Z}$. The results are plotted in Fig. 2.4 This result tells us that the flow in magnetic nozzle is stable regardless the velocity v_0 for constant velocity case. It is worth to mention $v_0 = 1$ is a singular point of this problem.

This solution is exact, we will use this to benchmark the simulation results in later chapter.

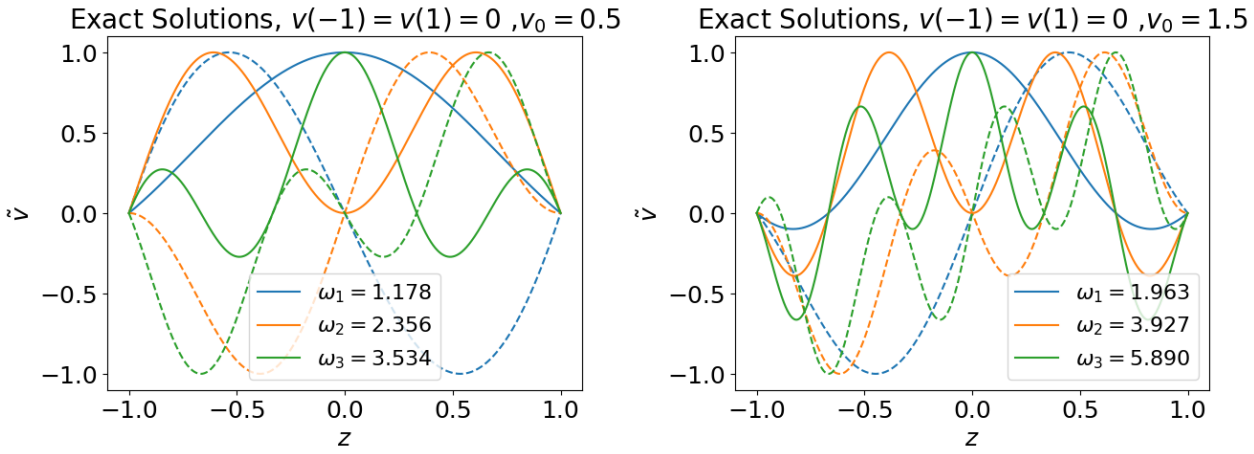

(a) Subsonic

(b) Supersonic

Figure 2.4: The plots show the first three non-zero exact solutions to Eq. (2.20) for both subsonic and supersonic case. These solutions are stable.

2.7.2 Fixed-Open Boundary

Fixed-Open boundary condition assumes that there are no perturbations at the entrance of the nozzle, and it is free on the exit of the nozzle.

$$\omega^2\tilde{v} + 2i\omega v_0\frac{\partial\tilde{v}}{\partial z} + (1-v_0^2)\frac{\partial^2\tilde{v}}{\partial z^2} = 0 \quad \tilde{v}(-1) = \frac{\partial\tilde{v}}{\partial z}(1) = 0 \tag{2.22}$$

The solution to this problem is

$$\tilde{v}(z) = C\left(\exp\left(i\omega\frac{z+1}{v_0+1}\right) - \exp\left(i\omega\frac{z+1}{v_0-1}\right)\right) \tag{2.23}$$

where $C \in \mathbb{C}$ is a complex constant, and $\omega = (v_0^2-1)\left[\frac{n\pi}{2} - \frac{1}{4}i\ln\left(\frac{v_0-1}{v_0+1}\right)\right]$ with $n \in \mathbb{Z}$. The term $i\ln((v_0-1)/(v_0+1)) \in \mathbb{C}$ and its imaginary part is positive for any $v_0 \neq 1$. Therefore,

- If $v_0 < 1$, then $\mathrm{Im}(\omega) < 0$, it's damped oscillation, hence stable.
- If $v_0 > 1$, then $\mathrm{Im}(\omega) > 0$, it's unstable.

Worth to mention, this is a very interesting solution with the following properties,

1. The growth rate is independent the mode number n.
2. The ground mode $n = 0$ for subsonic case has non-zero real part and imaginary part.

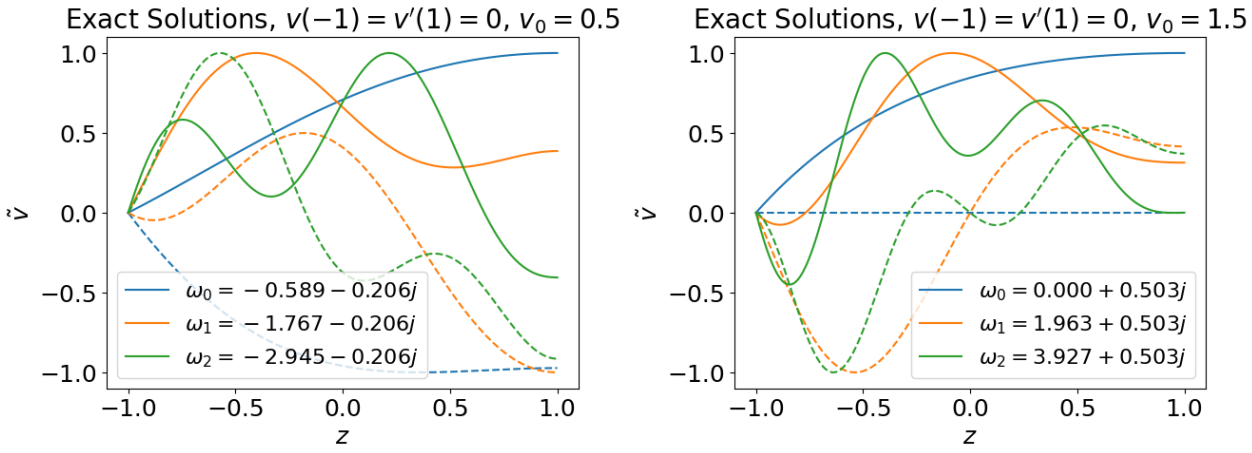

(a) Subsonic, stable flow.

(b) Supersonic, unstable flow.

Figure 2.5: The plots show the first three exact solutions to Eq. (2.22) for both subsonic and supersonic case. The flow is stable for subsonic case and unstable for supersonic case.

Chapter 3

Spectral Method

3.1 Spectral Theory in Finite-Dimensional Normed Spaces

Let X be a finite dimensional normed space and $\hat{T} : X \to X$ a linear operator. Since any linear operator can be represented by a matrix, the spectral theory of $\hat{T}$ is essentially matrix eigenvalue theory. [21] Let A be a matrix representation of $\hat{T}$, then we have the definition.

Definition 1. An eigenvalue of a square matrix A is a complex number λ such that

$$Ax = \lambda x$$

has a solution $x \neq 0$.This x is called an **eigenvector** of A corresponding to that eigenvalue λ.The set $\sigma(A)$ of all eigenvalues of A is called the **spectrum** of A. Its complement $\rho(A) = \mathbb{C} - \sigma(A)$ in the complex plane is called the **resolvent** set of A.

By choosing different bases in X, we can have different matrix representation of $\hat{T}$. We need to make sure the eigenvalues of a linear operator is independent of the basis chosen. Fortunately, a theorem ensures that.

Theorem 1. All matrices representing a given linear operator $\hat{T} : X \to X$ on a finite dimensional normed space X relative to various bases for X have the same eigenvalues.

Moreover, we don't need to worry about the existence of eigenvalues of a linear operator. The following theorem shows the existence of them.

Theorem 2. A linear operator on a finite dimensional complex normed space $X \neq O$ has at least one eigenvalue.

3.2 Spectral Theory in Normed Spaces of Any Dimension

Let $X \neq 0$ be a complex normed space (could be any dimension), and $\hat{T} : D(\hat{T}) \to X$ with domain $D(\hat{T}) \subset X$. Again, we could define eigenvalues, and other related concepts in terms of the equation

$$\hat{T}x = \lambda x$$

Definition 2. Let $\hat{T} \neq 0$ be a complex normed space and $\hat{T} : D(\hat{T}) \to X$ a linear operator with domain $D(\hat{T}) \subset X$. A **regular value** λ of $\hat{T}$ is a complex number such that

(R1) $(\hat{T} - \lambda I)^{-1}$ exists,

(R2) $(\hat{T} - \lambda I)^{-1}$ is bounded,

(R3) $(\hat{T} - \lambda I)^{-1}$ is defined on a set which is dense in X,

The **resolvent set** $\rho(\hat{T})$ of $\hat{T}$ is the set of all regular values λ of $\hat{T}$. Its complement $\sigma(\hat{T}) = \mathbb{C} - \rho(\hat{T})$ in the complex plane $\mathbb{C}$ is called the **spectrum** of $\hat{T}$, and a $\lambda \in \sigma(\hat{T})$ is called a **spectral value** of $\hat{T}$. Furthermore, the spectrum $\sigma(\hat{T})$ is partitioned into three disjoint sets as follows.

- The **point spectrum** or **discrete spectrum** $\sigma_p(\hat{T})$ is the set such that $(\hat{T} - \lambda I)^{-1}$ does not exist. A $\lambda \in \sigma_p(\hat{T})$ is called an **eigenvalue** of $\hat{T}$.
- The **continuous spectrum** $\sigma_c(\hat{T})$ is the set such that $(\hat{T} - \lambda I)^{-1}$ exists and satisfies (R3) but not (R2), that is, $(\hat{T} - \lambda I)^{-1}$ is unbounded.
- The **residual spectrum** $\sigma_r(\hat{T})$ is the set such that $(\hat{T} - \lambda I)^{-1}$ exists (and may be bounded or not) but does not satisfy (R3), that is, the domain of $(\hat{T} - \lambda I)^{-1}$ is not dense in X.

In practice, the eigenvalue problem in infinite dimension is difficult. Therefore, the usual approach to the eigenvalue problem $\hat{T}x = \lambda x$ is to first discretize the operator $\hat{T}$ to an approximated matrix operator T, then the eigenvalue problem becomes,

$$Tx = \lambda x$$

There are different ways to discretize the operator. For example, we can use finite difference, finite element and spectral element methods.

One important thing we need to keep in mind is that, the discretized version of the eigenvalue problem can have eigenvalues that are not in $\sigma(\hat{T})$. Those eigenvalues are called spurious eigenvalues, and this phenomenon is called spectral pollution. It is due to the improper discretization of the operators. We will discuss spectral pollution in the next section.

3.3 Different Discretizations

Spectral method is one of the best tools to solve PDE and ODE problems. [33] The central idea of spectral method is by discretizing the equation, we can transform that to a linear system or an eigenvalue problem.

Here we reformulate the polynomial eigenvalue problem, Eq. (2.19) as the following,

$$\begin{bmatrix} 0 & 1 \\ \hat{M} & \hat{N} \end{bmatrix} \begin{bmatrix} \tilde{v} \\ \omega\tilde{v} \end{bmatrix} = \omega \begin{bmatrix} \tilde{v} \\ \omega\tilde{v} \end{bmatrix} \tag{3.1}$$

where the operators $\hat{M}$ and $\hat{N}$ are defined as

$$\hat{M} = -\left[(1-v_0^2)\frac{\partial^2}{\partial z^2} - \left(3v_0 + \frac{1}{v_0}\right)\frac{\partial v_0}{\partial z}\frac{\partial}{\partial z} - \left(1 - \frac{1}{v_0^2}\right)\left(\frac{\partial v_0}{\partial z}\right)^2 - \left(v_0 + \frac{1}{v_0}\right)\frac{\partial^2 v_0}{\partial z^2}\right]$$
$$\hat{N} = -2i\left(v_0\frac{\partial}{\partial z} + \frac{\partial v_0}{\partial z}\right)$$

This becomes an ordinary algebraic eigenvalue problem if we discretize the operators and the function $\tilde{v}$. The following subsections discuss different discretizations of the problem.

3.3.1 Finite Difference

Consider equally spaced nodes on domain $[-1, 1]$, $\{x_1, x_2, \ldots, x_N\}$ with $x_{j+1} - x_j = h$ for each j, and the set of corresponding function values, $\{f_1, f_2, \ldots, f_N\}$. We can approximate the derivatives using second-order central difference formulas

$$\frac{\partial f}{\partial z} = \frac{f_{j+1} - f_{j-1}}{2h} \qquad \frac{\partial^2 f}{\partial z^2} = \frac{f_{j+1} - 2f_j + f_{j-1}}{h^2}$$

We can discretize the differentiation operators to the following matrices

$$\frac{\partial}{\partial z} \to D = \frac{1}{2h}\begin{bmatrix} 0 & 1 & 0 & \dots & 0 \\ -1 & \ddots & \ddots & \ddots & \vdots \\ 0 & \ddots & \ddots & \ddots & 0 \\ \vdots & \ddots & \ddots & \ddots & 1 \\ 0 & \dots & 0 & -1 & 0 \end{bmatrix} \qquad \frac{\partial^2}{\partial z^2} \to D^2 = \frac{1}{h^2}\begin{bmatrix} -2 & 1 & 0 & \dots & 0 \\ 1 & \ddots & \ddots & \ddots & \vdots \\ 0 & \ddots & \ddots & \ddots & 0 \\ \vdots & \ddots & \ddots & \ddots & 1 \\ 0 & \dots & 0 & 1 & -2 \end{bmatrix}$$

Using these differentiation matrices, Eq. (3.1) becomes

$$\begin{bmatrix} O & I \\ M & N \end{bmatrix}\begin{bmatrix} \tilde{\mathbf{v}} \\ \omega\tilde{\mathbf{v}} \end{bmatrix} = \omega\begin{bmatrix} \tilde{\mathbf{v}} \\ \omega\tilde{\mathbf{v}} \end{bmatrix} \tag{3.2}$$

where O is a zero matrix, I is an identity matrix, and

$$\begin{aligned} M =& -\operatorname{diag}(1-\mathbf{v}_0^2)D^2 + \operatorname{diag}\left(3\mathbf{v}_0 + \frac{1}{\mathbf{v}_0}\right)(D\mathbf{v}_0)D + \operatorname{diag}\left(1 - \frac{1}{\mathbf{v}_0^2}\right)(D\mathbf{v}_0)^2 \\ &+ \operatorname{diag}\left(\mathbf{v}_0 + \frac{1}{\mathbf{v}_0}\right)(D^2\mathbf{v}_0) \\ N =& -2i\left(\operatorname{diag}(\mathbf{v}_0)D + D\mathbf{v}_0\right) \end{aligned}$$

Here we abused the notation for the purpose of convenience, $\mathbf{v}_0^2$ means squaring every component of $\mathbf{v}_0$, and $1/\mathbf{v}_0$ denotes 1 divided by all components of $\mathbf{v}_0$.

Boundary Condition

We impose Dirichlet boundary condition on the problem, meaning that $\tilde{v}(-1) = \tilde{v}(1) = 0$. Further more, the differentiation matrices do not do well on the edges, so during the computation, we remove the first and last row of the differentiation matrices and the vectors $\tilde{\mathbf{v}}$ and $\mathbf{v}_0$. After the computation, we set $\tilde{v}_1 = \tilde{v}_N = 0$.

3.3.2 Spectral Element

Suppose the basis functions are $\{u_k(z)\}_{k=1}^{\infty}$, then the eigenfunction $\tilde{v}$ can be approximated by finite amount of them, $\tilde{v}(z) = \sum_{k=1}^{N} c_k u_k(z)$ where c_k are coefficients to be determined.

Then by multiplying u_i to any term and integrate through the domain, we can discretize the equation. Using the notation of inner product $(f, g) = \int_{-1}^{1} dz f g$, we see that

$$\int_{-1}^{1} dz\ u_i \tilde{v} = \sum_j (u_i, u_j) c_j$$

$$\int_{-1}^{1} dz\ u_i \frac{\partial \tilde{v}}{\partial z} = \sum_j \left(u_i, \frac{\partial u_j}{\partial z} \right) c_j$$

$$\int_{-1}^{1} dz\ u_i \frac{\partial^2 \tilde{v}}{\partial z^2} = \sum_j \left(u_i, \frac{\partial^2 u_j}{\partial z^2} \right) c_j$$

Suppose the basis functions are $\{u_k(z)\}_{k=1}^{\infty}$, then the eigenfunction $\tilde{v}$ can be approximated by finite amount of them, $\tilde{v}(z) = \sum_{k=1}^{N} c_k u_k(z)$ where c_k are coefficients to be determined.

$$\begin{bmatrix} O & I \\ M & N \end{bmatrix} \begin{bmatrix} \mathbf{c} \\ \omega \mathbf{c} \end{bmatrix} = \omega \begin{bmatrix} \mathbf{c} \\ \omega \mathbf{c} \end{bmatrix} \tag{3.3}$$

where O is a zero matrix, I is an identity matrix, and

$$M_{jk} = -\int_{-1}^{1} dz\ u_j \left[(1 - v_0^2) \frac{\partial^2}{\partial z^2} - \left(3v_0 + \frac{1}{v_0} \right) \frac{\partial v_0}{\partial z} \frac{\partial}{\partial z} - \left(1 - \frac{1}{v_0^2} \right) \left(\frac{\partial v_0}{\partial z} \right)^2 - \left(v_0 + \frac{1}{v_0} \right) \frac{\partial^2 v_0}{\partial z^2} \right] u_k$$

$$N_{jk} = -2i \int_{-1}^{1} dz\ u_j \left(v_0 \frac{\partial}{\partial z} + \frac{\partial v_0}{\partial z} \right) u_k$$

Boundary Conditions and Basis Function

To satisfy the Dirichlet boundary condition, $\tilde{v}(\pm 1) = 0$, we can choose a set of basis functions that satisfy the boundary condition $u_k(\pm 1) = 0, \forall k \in \mathbb{N}$. For example, the sine functions

$$u_n(z) = \sin\Big(\frac{n\pi}{2} (z + 1) \Big), n \in \mathbb{N}$$

is a set of basis functions that satisfy the Dirichlet boundary condition.

3.3.3 Finite Element

Finite-element method is a generalization of the spectral element method. We are allow to use a set of basis functions similar to spectral method in a cell. The region consists of many of these cells.

The formulation is the same as Eq. (3.3). The only difference is that in finite-element we need to solve Eq. (3.3) simultaneously for all cells.

Boundary Conditions and B-Spline

The B-Spline is a commonly used basis function for finite-element method. B-Spline can be defined recursively starting with piecewise constants [reference needed]

$$B_{i,0}(\xi) = \begin{cases} 1, & \text{if } \xi_i \leq \xi \leq \xi_{i+1} \\ 0, & \text{otherwise} \end{cases} \tag{3.4}$$

For $j \in \mathbb{N}$, they are defined by

$$B_{i,j}(\xi) = \frac{\xi - \xi_i}{\xi_{i+j} - \xi_i} B_{i,j-1}(\xi) + \frac{\xi_{i+j+1} - \xi}{\xi_{i+j+1} - \xi_{i+1}} B_{i+1,p-1}(\xi) \tag{3.5}$$

where $\xi = [\xi_0, \cdots, \xi_m]$ is called the knot vector, where $m = n + j + 1$ where $n + 1$ is the number of B-Splines and j is the degree of B-Spline polynomials. The knot vector defines the shapes of the B-Splines, see Fig. 3.1. The variable ξ is within the range $[\xi_0, \xi_m]$.

Any function $u(x)$ on $[\xi_0, \xi_N]$ can be approximated by

$$u(x) \simeq \sum_{j=0}^{n} c_j B_{i,j}(x)$$

The Dirichlet boundary condition can be set by letting the coefficients of the first and last B-Spline to 0, $c_0 = c_n = 0$, where N is the number of B-Splines.

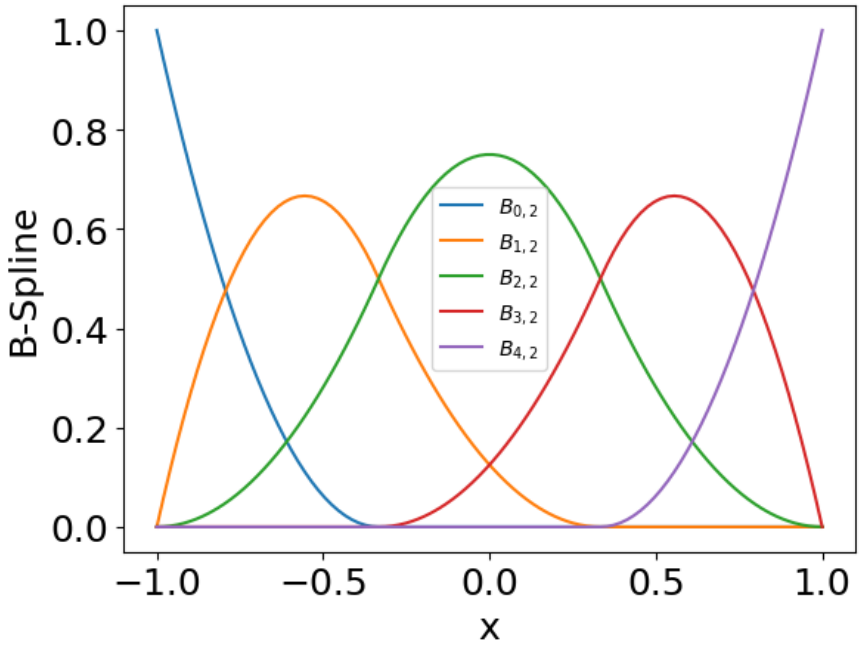

Figure 3.1: An example of open uniform quadratic B-Spline on $[-1, 1]$. The knot vector is [-1,-1,-1,-1/3,1/3,1,1,1].

3.4 Spectral Pollution and Spurious Modes

In this section, we will discuss an important phenomenon we observe throughout the numerical experiments. It is the phenomenon of spectral pollution. Then we will provide a method to filter these spurious modes.

Spectral pollution refers to the phenomenon which some eigenvalues are not converging to the correct value when the mesh density is increased. When solving eigenvalue problems using spectral methods with finite difference or finite element approximations, spectral pollution might occur. [24]

3.4.1 Finite Difference Discretization of Operators

In this section, we are going to investigate the spectral pollution phenomenon when solving Eq. (2.20) using spectral method.

The dispersion relation can be obtained by substituting $\tilde{v} = \exp(-i\omega t + kx)$ into Eq. (2.20),

$$\omega = k(v_0 \pm 1) \tag{3.6}$$

If we assume $v \sim \exp(ikx)$, and let $\beta \equiv kh/2$. Then in finite difference discretization

scheme, the differential operators $\mathrm{d}^n/\mathrm{d}z^n$ are equivalent to the following factors [24],

$$\begin{aligned} G_0 &= 1 \\ G_1 &= [\exp(2i\beta) - \exp(-2i\beta)]/2h = (i/h)\sin(2\beta) \\ G_2 &= [\exp(2i\beta) - 2 - \exp(-2i\beta)]/h^2 = (2/h^2)(\cos(2\beta) - 1) \end{aligned} \tag{3.7}$$

3.4.2 Analysis of Numerical Spectrum

Discretize on the Same Grid

Using the G-operator, Eq. (3.7), the discretized equation of Eq. (2.20) is

$$(\omega^2 G_0 + \omega G_1 + G_2)\tilde{\mathbf{v}} = 0 \tag{3.8}$$

where $\tilde{\mathbf{v}}$ is the discretized vector of $\tilde{v}$.

Solving Eq. (3.8), we obtain the numerical dispersion relation,

$$\omega = \frac{2\sin(\beta)}{h}\left(v_0 \pm \sqrt{1 - v_0^2\sin^2(\beta)}\right) \tag{3.9}$$

Given h (fixed the mesh resolution), we see that

- ω is real for all k if $v_0 < 1$.
- ω is complex for large k, more specifically $k > h/2\arcsin(1/v_0)$, if $v_0 > 1$.
- For small k, meaning $k \to 0$, Eq. (3.9) is a good representation for the analytical dispersion relation, Eq. (3.6).

This explains why the spurious unstable modes occur when $v_0 > 1$.

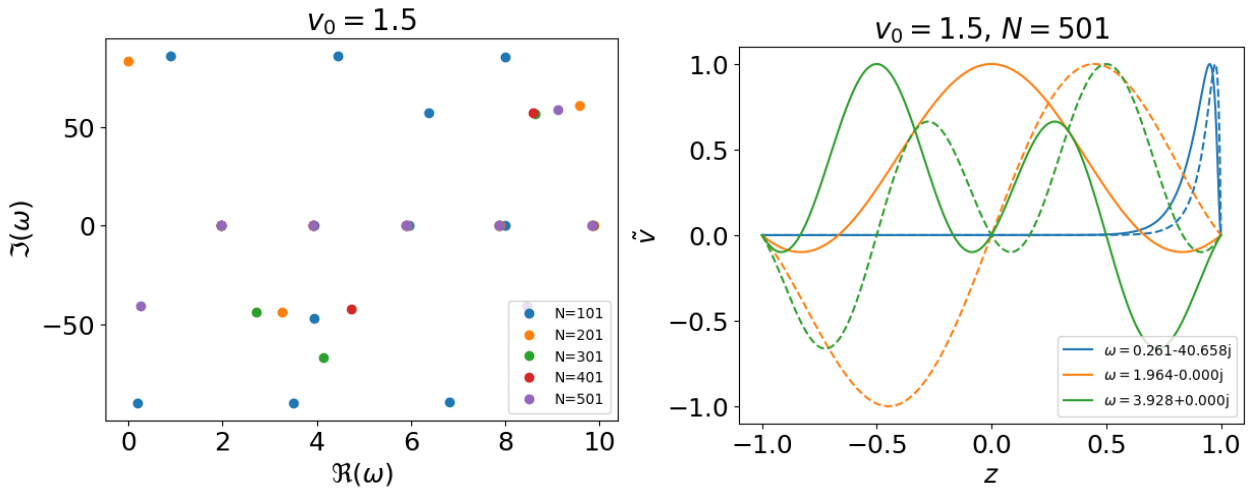

(a) Bad eigenvalues

(b) Bad eigenfunctions

Figure 3.2: Spurious modes.

One way to filter the spurious modes is to remove all modes with $k > h/2 \arcsin(1/v_0)$, see Fig. 3.3. However, this is not a good way to deal with general cases because it requires the solution to the discretized problem Eq. (3.8). For general problem with non-constant velocity profile, it is hard to solve the discretized problem directly.

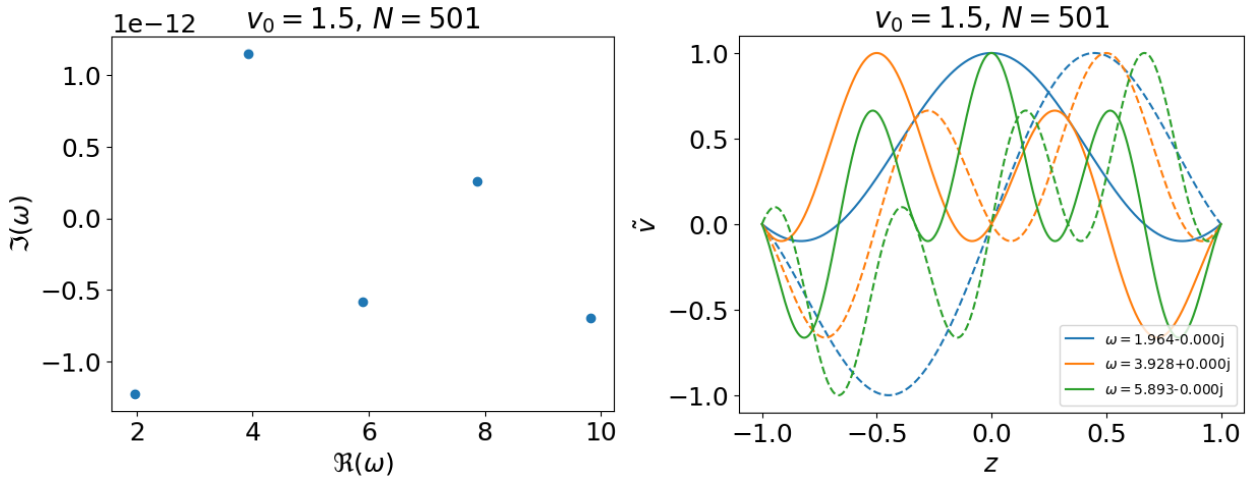

(a) Good eigenvalues

(b) Good eigenfunctions

Figure 3.3: Filter out the spurious modes with $k > h/2 \arcsin(1/v_0)$.

A better way to filter the spurious modes is by doing a "convergence test". Since the frequency Eq. (3.9) is changing with mesh resolution h. We can simply solve the discretized problem using spectral method under different mesh resolution. Then filter out the eigenmodes that are changing dramatically.

Chapter 4

Singular Perturbation

This chapter is dedicated to analyze the polynomial eigenvalue problem with transonic velocity profiles. We will first show the existence of the singularity of Eq. (2.19), then we will discuss the concept of singular perturbation and the way we solve the problem.

4.1 Presence of Singularity in Transonic cases

In order to see the existence of the singularity, we rearrange the terms the polynomial eigenvalue problem, Eq. (2.19),

$$\begin{aligned} &(1-v_0^2)\frac{\partial^2\tilde{v}}{\partial z^2} \\ &+\left[2i\omega v_0-\left(3v_0+\frac{1}{v_0}\right)\frac{\partial v_0}{\partial z}\right]\frac{\partial\tilde{v}}{\partial z} \\ &+\left[\omega^2+2i\omega\frac{\partial v_0}{\partial z}-\left(1-\frac{1}{v_0^2}\right)\left(\frac{\partial v_0}{\partial z}\right)^2-\left(v_0+\frac{1}{v_0}\right)\frac{\partial^2 v_0}{\partial z^2}\right]\tilde{v} \\ &=0 \end{aligned} \tag{4.1}$$

This is a second order ordinary differential equation defined on region $[-1,1]$.

For transonic (accelerating and decelerating) velocity profiles (Fig. 2.3), the plasma flow is at sonic point at the throat of the nozzle, $v_0(0)=1$. Therefore, the highest order term vanishes at $z=0$. This causes the failure of spectral method, see Fig. (6). It can be proved that $z=0$ is a regular singular point.

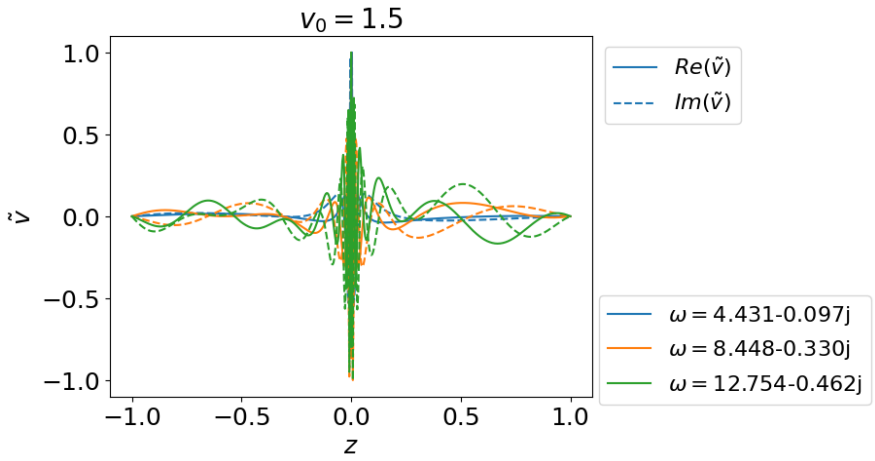

Figure 4.1: An attempt to solve the polynomial eigenvalue problem, Eq. (2.19) using finite-difference. Eigenfunctions are squeezed to the center of the nozzle due to the existence of the singularity at $z = 0$.

4.2 Connection of Transonic fluid Flow to Black Hole

Consider a transonic fluid flow, the sound waves can propagate from the subsonic region into the supersonic region, while propagating in the opposite direction is not allowed. This process is similar to masses falling into the black hole. Therefore, the sonic point of a transonic flow is an acoustic equivalent of event horizon of a black hole. Hence, a transonic flow is sometimes called an acoustic black hole. [26]

4.2.1 The Schrödinger-Type Wave Equation

In de Labal nozzle, the governing equations for quasi-one-dimensional flow of a perfect fluid are

$$\frac{\partial \rho A}{\partial t} + \frac{\partial \rho v A}{\partial z} = 0 \tag{4.2}$$

$$\rho \frac{\partial v}{\partial t} + \rho \frac{\partial v}{\partial z} = -\frac{\partial p}{\partial z} \tag{4.3}$$

$$p = \rho^{\gamma} \tag{4.4}$$

where ρ is the density, v is the velocity, p is the pressure, A is the cross section of the nozzle, and $\gamma = 1.4$ is the heat capacity ratio for air. The governing equations, Eq. (4.2), (4.3), and (4.4) above are conservation of density, momentum and energy, respectively.

We can reduce Eq. (4.3) to Bernoulli's equation

$$\frac{\partial \Phi}{\partial t} + \frac{1}{2}\left(\frac{\partial \Phi}{\partial z}\right)^2 + h(\rho) = 0 \tag{4.5}$$

where $h(\rho) = \int \rho^{-1} dp$ is the specific enthalpy and $\Phi = \int v dz$ is the velocity potential.

Now, we introduce the acoustic analogy of tortoise coordinate and a new function $H_\omega(z)$,

$$z^* = c_{s0} \int \frac{dz}{c_s(1 - M^2)}$$

$$H_\omega(z) = g^{1/2} \int dt e^{i\omega[t - f(z)]} \phi(t, x)$$

where $c_s = \sqrt{\gamma p/\rho}$, c_{s0} is the stagnation sound speed, it is a constant over isentropic region, $M = v/c_s$ is the Mach number, $g = \rho A/c_s$ and

$$f(x) = \int \frac{|v| dz}{c_s^2 - v^2}$$

If we perturb the density and the velocity potential by $\delta\rho$ and ϕ, respectively. Then employ the acoustic analogy of tortoise coordinate, the linearized wave equation for sounds can be transformed to a Schrödinger-type wave equation,

$$\left[\frac{\mathrm{d}^2}{\mathrm{d}z^{*2}} + \kappa^2 - V(z^*)\right] H_\omega = 0$$

where ω is the oscillating frequency of the perturbation, $\kappa = \omega/c_{s0}$ is the normalized frequency, and the effective potential

$$V(z^*) = \frac{1}{g^2}\left[\frac{g}{2}\frac{\mathrm{d}^2 g}{\mathrm{d}z^{*2}} - \frac{1}{4}\left(\frac{\mathrm{d}g}{\mathrm{d}z^*}\right)^2\right]$$

The effective potential $V(z^*)$ has dimension of $(\text{length})^{-2}$ and characterizes the "curvature scattering" of sound waves on the acoustic black hole. [26] By employing the acoustic tortoise coordinate, the singularity at the sonic point is pushed to infinity. When doing numerical simulations, we can solve the Schrödinger-type equation separately in subsonic and supersonic region of the nozzle.

It turns out, scalar field perturbations in the minimally geometric deformed brane-world

black hole background yields a very similar wave-like equation, [10]

$$\left[\frac{\mathrm{d}^2}{\mathrm{d}r^{*2}} + \omega^2 - V(r^*)\right]\Psi(r^*) = 0$$

where r^* is the tortoise coordinate.

4.3 Singular Perturbation Problem

In the previous section, we introduced transonic fluid flow as an acoustic analogy of black hole and transformed the Eq. 4.5 to a Schrödinger-type wave equation. This is an overkill for our problem. In this section, we will introduce a simpler way to deal with the singularity.

Consider Eq. (2.19) as a boundary value problem by fixing the value of ω, The boundary value problem Eq. (4.1) is defined on region $[-1, 1]$, but the boundary values are defined on $z = -1$ and $z = 0$. This is because to extract a regular solution near the singularity, we need to assume the solution is finite at the throat of the nozzle, $z = 0$. This condition serves as a boundary value to the problem. Together with the boundary condition at the entrance of the nozzle, $\tilde{v}(-1) = 0$, the solutions to the boundary value problem, Eq. (4.1) is fully determined up to a set of eigenvalues.

As we discuss in the earlier section, Sec.4.1, $(1 - v_0^2)$ is 0 at the nozzle throat $z = 0$ since $v_0(z)$ is now a transonic velocity profile. This makes the problem a first order ordinary differential equation,

$$\left(2i\omega - 4\left.\frac{\partial v_0}{\partial z}\right|_{z=0}\right)\frac{\partial \tilde{v}}{\partial z} + \left[2i\omega\left.\frac{\partial v_0}{\partial z}\right|_{z=0} - 2\left.\frac{\partial^2 v_0}{\partial z^2}\right|_{z=0}\right]\tilde{v} = 0$$

It is clear that the solution to this first order ODE has a totally different characteristics than the solution in the neighborhood of $z = 0$. That means we cannot simply set $(1 - v_0^2)$ to 0 and get an asymptotic approximation to the solution of Eq. (4.1) near $z = 0$. This is exactly the characteristics of singular perturbation problem.

4.4 Expansion at Singularity

The singularity is a regular singular point, we are able to extract finite solution near the singularity. In order to do so, we need to expand terms in Eq. (4.1) about the singularity.

The first task is to linearize the terms with v_0 about the singularity. The linearization of $v_0(z) = 1 + v_0'(0)z$ is a good approximation to the original function $v_0(z)$ because the transonic velocity profiles are straight in the neighborhood of $z = 0$, as we can see from

Fig. 2.3. Therefore, through some simple algebra we obtain,

$$\begin{aligned} 1 - v_0^2 &= -2v_0'(0)z \\ 3v_0 + \frac{1}{v_0} &= 4 + 2v_0'(0)z \\ 1 - \frac{1}{v_0^2} &= 2v_0'(0)z \\ v_0 + \frac{1}{v_0} &= 2 \end{aligned} \tag{4.6}$$

Then Eq. (4.1) becomes

$$\begin{aligned} &-2v_0'(0)z\frac{\partial^2\tilde{v}}{\partial z^2} \\ &+[2i\omega - 4v_0'(0) + (2i\omega - 2v_0'(0))z]\frac{\partial\tilde{v}}{\partial z} \\ &+\left[\omega^2 + 2i\omega v_0'(0) - 2v_0''(0) - 2v_0'(0)^3 z\right]\tilde{v} = 0 \end{aligned} \tag{4.7}$$

In fact, we can further simply the equation by dropping all z terms except the first term (second-order derivative term). It can be shown that dropping the z terms in Eq. (4.7) does not affect the first order correction ($\tilde{v}$ is the same up to z term), it is an acceptable approximation.

$$-2v_0'(0)z\frac{\partial^2\tilde{v}}{\partial z^2} + (2i\omega - 4v_0'(0))\frac{\partial\tilde{v}}{\partial z} + (\omega^2 + 2i\omega v_0'(0) - 2v_0''(0))\tilde{v} = 0$$

Dividing by the first coefficient, we have

$$z\frac{\partial^2\tilde{v}}{\partial z^2} + a\frac{\partial\tilde{v}}{\partial z} + b\tilde{v} = 0 \tag{4.8}$$

where

$$a = \frac{2i\omega - 4v_0'(0)}{-2v_0'(0)}; \quad b = \frac{\omega^2 + 2i\omega v_0'(0) - 2v_0''(0)}{-2v_0'(0)}$$

Use Frobenius method, we assume the velocity perturbation can be written as a power series in z, $\tilde{v} = \sum_{n\geq 0} c_n z^{n+r}$. By substituting the power series into Eq. (4.8) we have

$$\sum_{n\geq 0}(n+r)(n+r+1)c_n z^{n+r-1} + a(n+r)c_n z^{n+r-1} + bc_n z^{n+r} = 0$$

Shift the power of the last term we get

$$\sum_{n\geq 0}(n+r)(n+r+1)c_n z^{n+r-1} + a(n+r)c_n z^{n+r-1} + \sum_{n\geq 1} bc_{n-1} z^{n+r-1} = 0$$

Setting $n = 0$, we get the indicial equation

$$c_0 r(r-1) + c_0 ar = 0 \Rightarrow c_0 r(r+a-1) = 0$$

We get two different roots, $r = 0$ and $r = 1 - a$. They correspond to finite solution and diverging solution near the singularity, respectively.

The coefficients are given by recurrence relation

$$(n+r)(n+r-1)c_n + a(n+r)c_n + bc_{n-1} = 0 \Rightarrow c_n = \frac{-bc_{n-1}}{(n+r)(n+r-1+a)}$$

Solving this relation we get explicit expression for c_n, $n \in \mathbb{N}$,

$$\begin{aligned} c_n &= \frac{(-1)^n b^n c_0}{\prod_{k=0}^{n-1}(n+r-k)(n+r-1+a-k)} \\ &= (-1)^n b^n c_0 \frac{\Gamma(r+1)\Gamma(r+a)}{\Gamma(n+r+1)\Gamma(n+r+a)} \end{aligned} \tag{4.9}$$

Therefore, we successfully extracted the regular solution (corresponding to the root $r = 0$) in the form of power series,

$$\begin{aligned} \tilde{v} &= c_0 + c_1 z + c_2 z^2 + \cdots \\ &= c_0 - c_0 \frac{b}{a} z + c_0 \frac{b^2}{2a(1+a)} z^2 + \cdots \end{aligned} \tag{4.10}$$

It is worth to mention that the diverging solution (corresponding to the root $r = a$) goes like

$$\tilde{v}(z) \sim z^{1-a} = z^{-1-\omega_i/v_0'(0)} z^{i\omega_r/v_0'(0)}$$

where $\omega = \omega_r + i\omega_i$. Meaning that the divergent solution will start to diverge when $\omega_i > -v'(0)$.

4.5 Shooting Method

Shooting method can be used to solve eigenvalue problem with specified boundary values,

$$g(\tilde{v}(z); \omega) = 0, \quad z_l \le z \le z_r, \quad \tilde{v}(z_l) = \tilde{v}_l, \tilde{v}(z_r) = \tilde{v}_r \tag{4.11}$$

where ω is the eigenvalue to be solved.

Suppose an eigenvalue problem can be formulated as

$$\frac{\mathrm{d}}{\mathrm{d}z}\mathbf{u} = \mathbf{f}(\mathbf{u}, z; \omega), \quad z_l < z < z_r, \quad \mathbf{u}(z_l) = \mathbf{u}_l$$

where $\mathbf{u} \in \mathbb{R}^2$. Fixed an ω, we can approximate $\mathbf{u}(z_r)$ by applying algorithms such as Runge-Kutta or Leap-frog.

Define F by $F(\mathbf{u}_l; \omega) = \tilde{v}(z_r; \omega)$. This function F takes in the initial value $\mathbf{u}_l$ and a fixed ω, and outputs the "landing point" $\tilde{v}(z_r; \omega)$. If ω is an eigenvalue of Eq. (4.11), then $\tilde{v}(z_r; \omega) = \tilde{v}_r$. Now we can find eigenvalues to Eq. (4.11) by solving the roots to the scalar equation

$$h(\omega) = F(\mathbf{u}_l; \omega) - \tilde{v}_r$$

Having this higher view of shooting method in mind, we first transform Eq. (2.19) to a IVP,

$$\begin{aligned} v' &= u \\ u' &= \frac{-1}{1 - v_0^2}\left[\omega^2 v + 2i\omega(v_0 + v_0' v) - \left(3v_0 - \frac{1}{v_0}\right) v_0' u - \left(1 - \frac{1}{v_0}^2\right)(v_0')^2 v - \left(v_0 + \frac{1}{v_0} v_0''\right) v\right] \end{aligned}$$

and $v(0) = c_0 = 1, u(0) = c_1 = (2i\omega v_0' - 2v_0'')/2v_0'$. Moreover, $u'(0) = c_2 = -((v_0')^4 + (2i\omega v_0' + (v_0')^2 - v_0'')(i\omega v_0' - v_0''))/(v_0'(2i\omega - 6v_0'))$.

In order to get initially value for cases with transonic velocity profiles, we need to expand the solution at the singularity.

Chapter 5

Numerical Experiments

In this chapter, we will solve the eigenvalue problem, Eq. (3.1), with different discretizations. There will be three major categories of methods used. Finite difference (FD) method, finite element (FE) method and spectral element method (SE).

The finite difference method will be used together with equally spaced nodes. The finite element method will use B-spline as basis functions. Finally, the spectral element method uses sine functions as the spectral elements.

For Dirichlet boundary, The parameters of different discretizations are listed below

Table 5.1: With Dirichlet boundary condition, all methods have good accuracy, so using 101 nodes in the region $[0, 1]$ is enough. For FE and SE methods, they are using 50 basis functions.

	FD	FE_BSPLINE	SE_SINE
N	101	101	101
NUM_BASIS		51	50

For left-fixed and right-open (fixed-open) boundary condition, the parameters are

Table 5.2: With fixed-open boundary condition, it requires higher resolution in order to get accurate results. Therefore all methods use 501 nodes in the region $[0, 1]$, and FE method uses 101 basis functions.

	FD	FE_BSPLINE
N	501	501
NUM_BASIS		101

5.1 Constant Velocity Case

5.1.1 Dirichlet Boundary

Because the existence of exact solution to problems Eq. (2.20). The case with constant velocity profile is used as a sanity check. It allows us to verify the correctness of each method's implementation. This also serves as a reference to the accuracy spectral methods can achieve.

From Fig. (5.1), we see that the order of growth rates obtained by different methods is about 10^{-14} for both subsonic and supersonic cases. We will use these numbers as a reference to the accuracy of our numerical methods. If a method produces growth rates with order close to 10^{-14}, we consider the growth rates to be 0.

Table 5.3: Relative error of each eigenvalue.

$v_0 = 0.5$	1	2	3	4	5
FD	2.827e-05	1.130e-04	2.541e-04	4.512e-04	7.040e-04
FE	0.005	0.005	0.006	0.008	0.010
SE	2.896e-05	1.157e-04	2.603e-04	4.626e-04	7.217e-04

$v_0 = 1.5$	1	2	3	4	5
FD	0.001	0.005	0.010	0.019	0.030
FE	0.006	0.010	0.019	0.029	0.043
SE	0.001	0.005	0.011	0.019	0.030

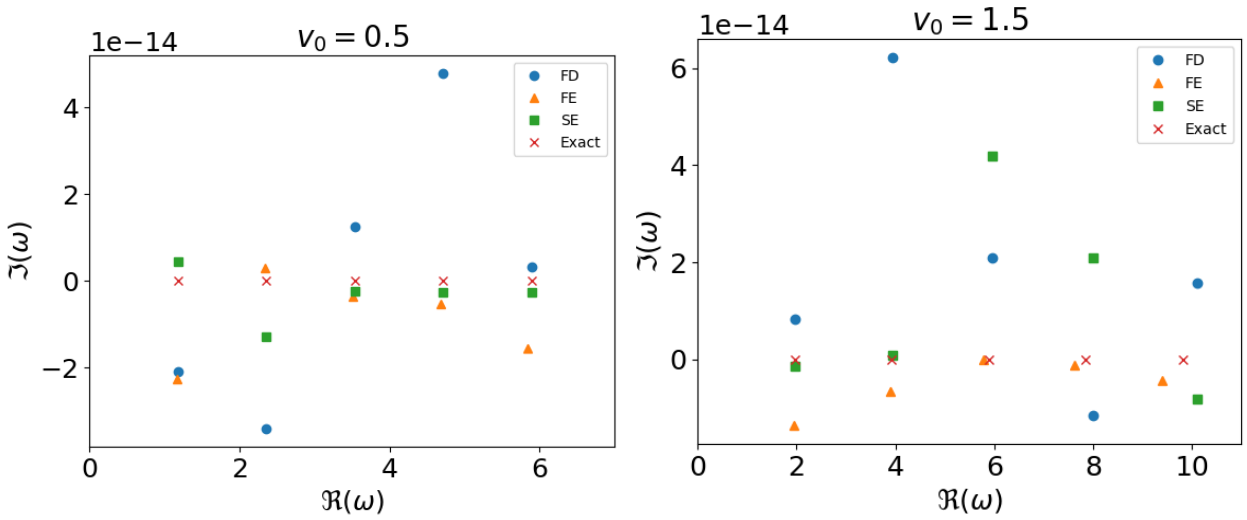

(a) All modes are stable.

(b) Filtered modes are stable.

Figure 5.1: Showing the first 5 eigenvalues of each method in each case. All methods are close to the exact eigenvalues.

5.1.2 Fixed-Open Boundary

Table 5.4: Relative error of each eigenvalue. Notice that the ground mode for subsonic case is non-zero.

$v_0 = 0.5$	0	1	2	3	4
FD	1.209e-05	3.458e-05	5.775e-05	8.153e-05	1.061e-04
FE	8.090e-05	2.007e-04	2.981e-04	6.596e-04	1.821e-03
$v_0 = 1.5$	1	2	3	4	5
FD	9.163e-05	2.435e-04	4.833e-04	8.160e-04	1.243e-03
FE	4.431e-04	7.924e-04	1.516e-03	3.103e-03	8.001e-03

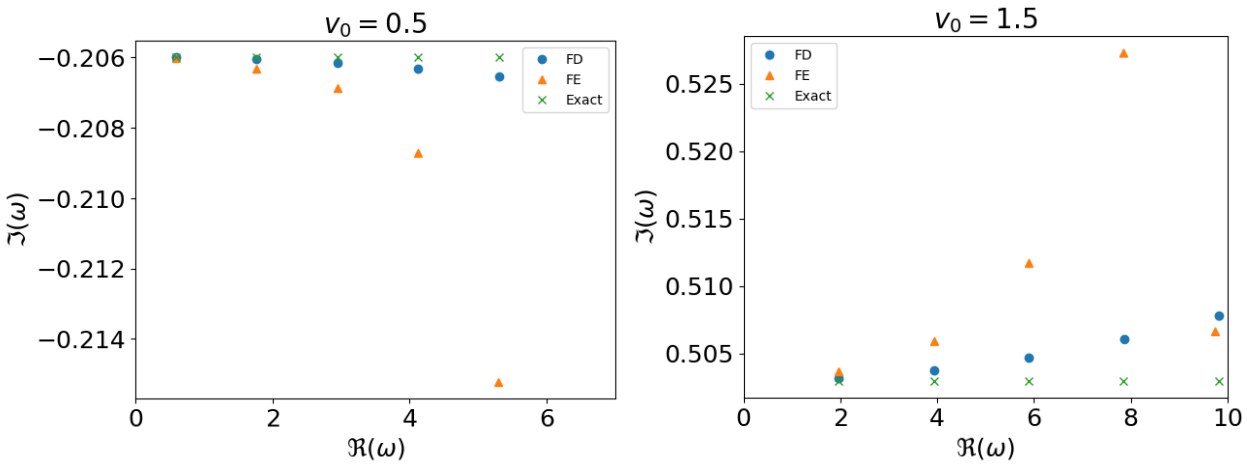

(a) All modes are stable.

(b) All modes are unstable.

Figure 5.2: Showing the first 5 eigenvalues of each method. Finite-difference method has much better accuracy than finite-element method.

5.2 Subsonic Case

5.2.1 Dirichlet Boundary

When setting the mid-point velocity to be $M_m = 0.5$, we have the subsonic velocity profile. This velocity profile is the orange line shown in Fig. 2.3. With Dirichlet boundary condition, $\tilde{v}(\pm 1) = 0$. The flow in magnetic nozzle is stable. Fig. 5.3 shows the first few eigenvalues obtained by different discretizations.

The order of growth rates obtained by different methods is 10^{-13}, we can consider it to be stable.

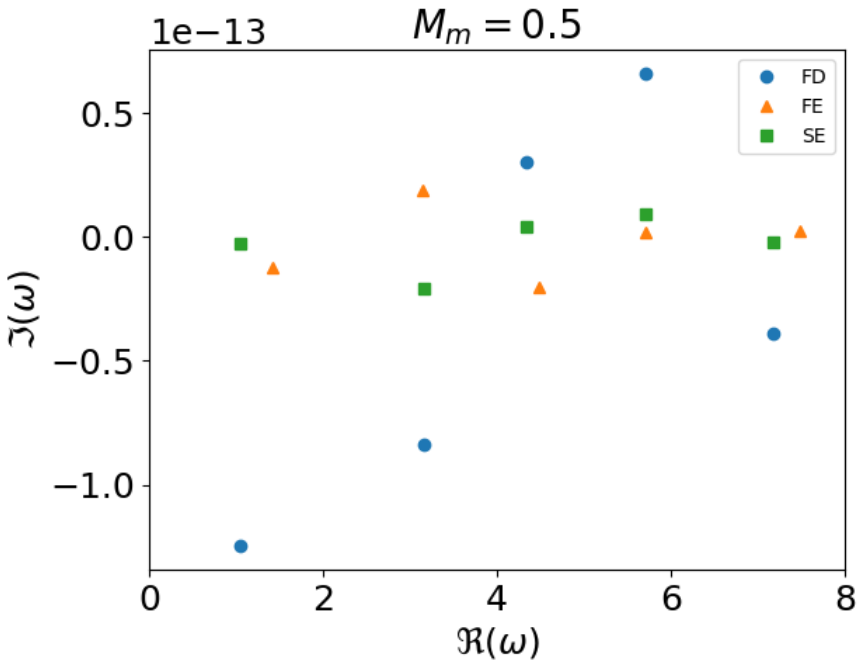

Figure 5.3: Showing the first 5 modes. It suggests that the flow in magnetic nozzle with subsonic velocity profile and Dirichlet boundary condition is stable.

5.2.2 Fixed-Open Boundary

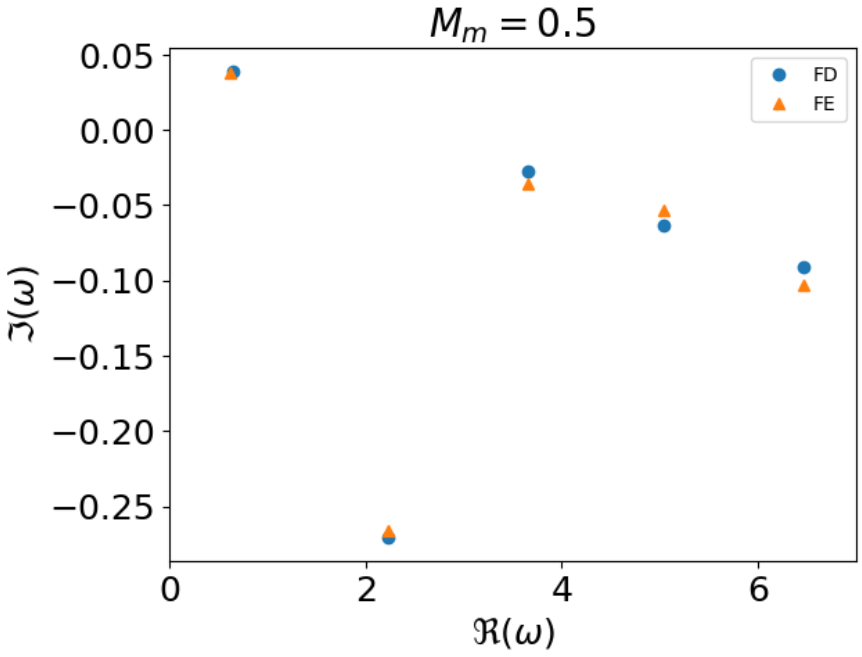

Figure 5.4: Showing the first 5 modes. The ground mode is unstable, other modes are stable.

5.3 Supersonic Case

5.3.1 Dirichlet Boundary

When the velocity profile is supersonic, shown as purple line in Fig. 2.3, spurious modes appeared as predicted in Chap. 2. Using the convergence test, we successfully eliminates all unstable modes. Fig. (5.5) shows the first few filtered eigenvalues. As we can see the flow is stable.

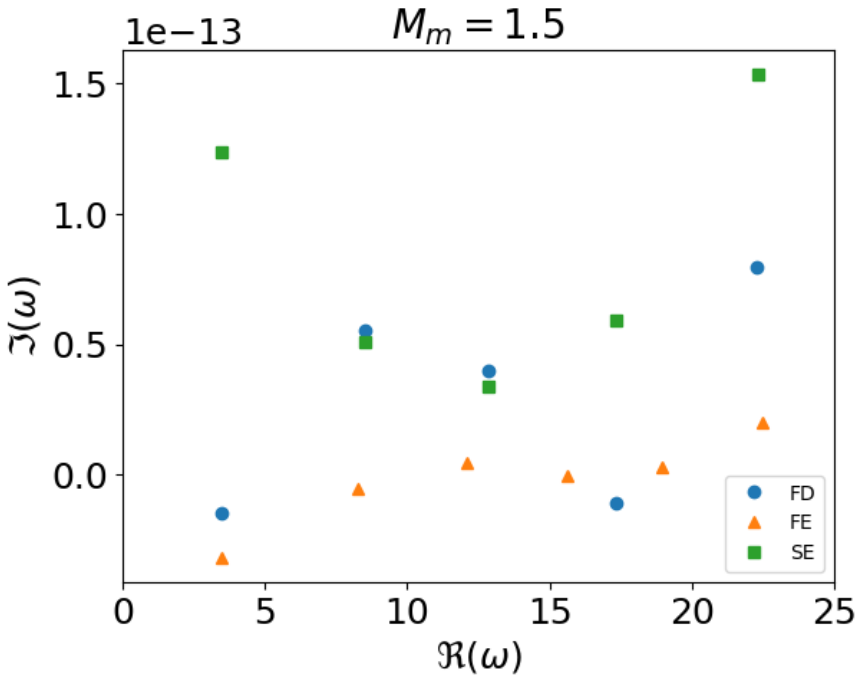

Figure 5.5: First few filtered eigenvalues are shown. The spurious modes are filtered by convergence test.

5.3.2 Fixed-Open Boundary

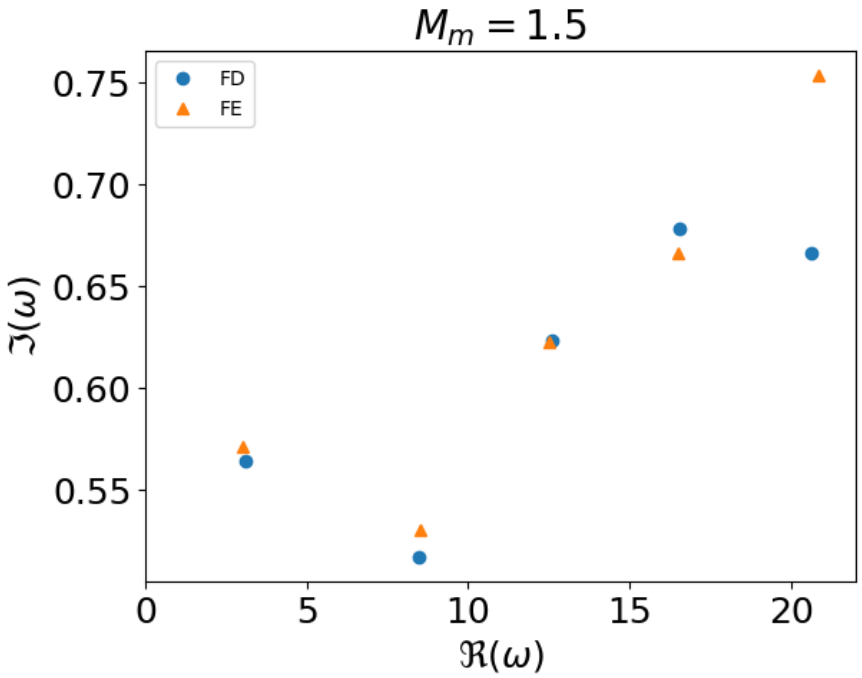

Figure 5.6: All modes are unstable.

5.4 Accelerating Case

Starting from the singular point, we shoot the solution to the left boundary. We find the set of eigenvalues such that $\tilde{v}(-1) = 0$. With these eigenvalues, we can extend the solution to the supersonic region $(0, 1]$. The first few eigenmodes are drawn in Fig. 5.7.

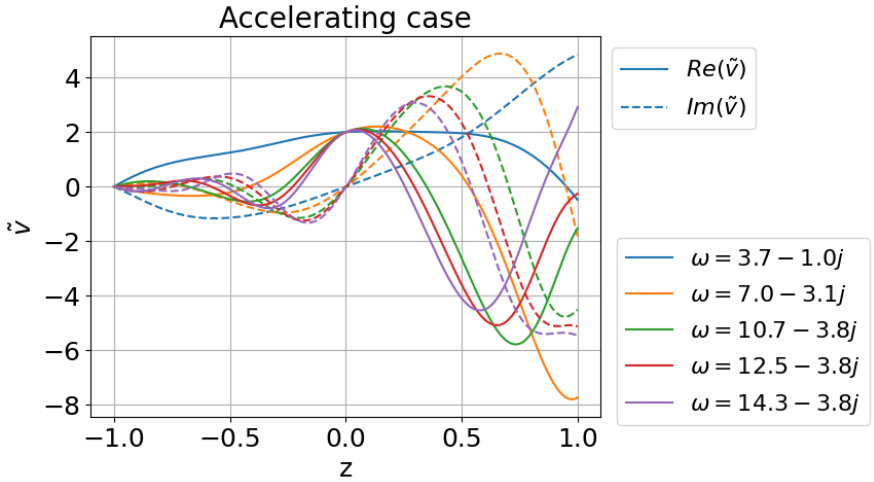

Figure 5.7: The eigenmodes are stable.

5.5 Decelerating Case

Again, we set the perturbations at the entrance of the nozzle to 0, $\tilde{v}(-1) = 0$. Then we apply the same procedure as accelerating case, we obtained the following Fig. 5.8. The results indicates that the decelerating case is physically impossible with the selected boundary condition.

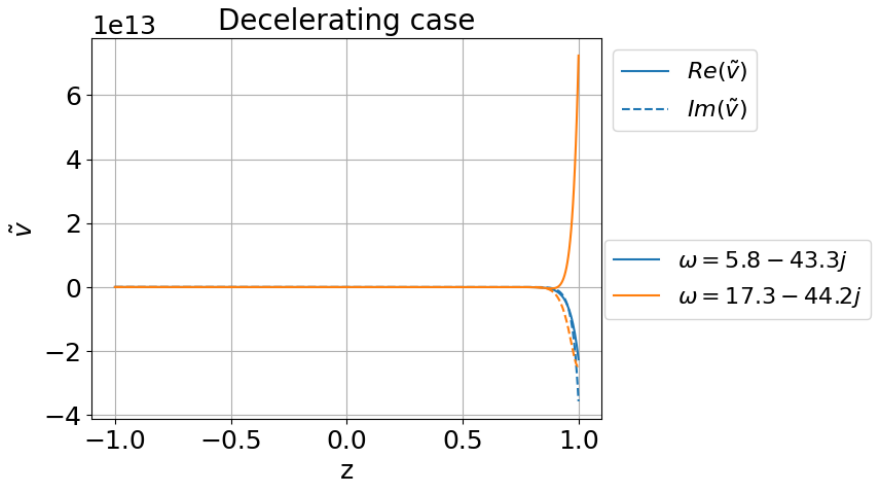

Figure 5.8: The perturbations at the exit of the nozzle explode. It is not physically possible, therefore the decelerating case might not be physically with the given boundary condition.

Chapter 6

Discussion

6.1 Summary of the Results

For the subsonic flow, it is stable under Dirichlet boundary condition. It is also stable under fixed-open boundary, except for ground mode when velocity is nonuniform. For the supersonic flow, it is stable when Dirichlet boundary condition is applied, and unstable is the boundary condition is fixed-open. The results are summarized in Table. 6.1.

The flow with accelerating velocity profile is stable, assuming there is no velocity perturbation at the entrance of the nozzle. On the other hand, the decelerating flow is physically impossible under the boundary condition where velocity perturbation is 0 at the entrance. The results are summarized in Table. 6.2.

	Subsonic	Supersonic
Dirichlet	Stable	Stable
Fixed-Open	Stable (except ground mode if velocity is non-uniform)	Unstable

Table 6.1: The Dirichlet boundary condition means there are no perturbations at the two ends of the nozzle. While the fixed-open condition assume that there is no perturbation at the entrance of the nozzle, $\tilde{v}(-1) = 0$, and then the derivative with respect to z of the velocity perturbation is 0 at the exit, $\partial_z \tilde{v}(1) = 0$.

Accelerating	Decelerating
Stable	Impossible

Table 6.2: The boundary condition is set so that there is no perturbation at the entrance of the nozzle, $\tilde{v}(-1) = 0$, and then reaches a finite value at the throat of the nozzle, $\tilde{v}(0) = 1$.

6.2 Limitations of the methods

6.2.1 Spectral Method

The spectral method suffers the spectral pollution. For now there is no automatic ways to filter spurious modes other than doing convergence test and pick up the convergent eigenvalues manually by ourselves. We believe there is a discretization scheme that is spectral pollution free. In fact, we made optimistic guess based on the fact that normal form of Eq. (2.19) with constant velocity profile is pollution free.

6.2.2 Shooting Method

The shooting method is not exhaustive due to the nature of root finding algorithm. A root can only be found if the initial guess of the root is close enough to the actual root. To work around this issue, we have to perform a grid search on the complex plane. This way we can only survey the low frequency region due to the finiteness of computing resources. The conclusion for cases with transonic velocity profiles is true only for low frequency region.

6.3 Conclusion

In Chap. 2, we derived the linearized equations of motion of the flow in one dimensional magnetic nozzle. Furthermore, we rewrite the linearized governing equations as an eigenvalue problem. Using the spectral methods introduced in chapter 2, we discretized the operators of the problem. Hence, transforming it into an algebraic eigenvalue problem.

With the aid of computer, we are able to solve the algebraic eigenvalue problem. The results show that the flow in magnetic nozzle with Dirichlet boundary condition is stable except the case with decelerating velocity profile.

Bibliography

[1] Cpep - contemporary physics education project. Accessed: March 26, 2024.

[2] Toshiki Aikawa. The stability of spherically symmetric accretion flows. *Astrophys Space Sci*, 66(2):277–285, December 1979.

[3] S. A. Andersen. Continuous Supersonic Plasma Wind Tunnel. *Phys. Fluids*, 12(3):557, 1969.

[4] H. Bondi. On Spherically Symmetrical Accretion. *Monthly Notices of the Royal Astronomical Society*, 112(2):195–204, April 1952.

[5] R. W. Boswell, O. Sutherland, C. Charles, J. P. Squire, F. R. Chang Díaz, T. W. Glover, V. T. Jacobson, D. G. Chavers, R. D. Bengtson, E. A. Bering, R. H. Goulding, and M. Light. Experimental evidence of parametric decay processes in the variable specific impulse magnetoplasma rocket (VASIMR) helicon plasma source. *Physics of Plasmas*, 11(11):5125–5129, November 2004.

[6] Lyonell Boulton. Spectral pollution and eigenvalue bounds. *Applied Numerical Mathematics*, 99:1–23, January 2016.

[7] Richard L Burden, J Douglas Faires, and Annette M Burden. *Numerical Analysis*. 2016.

[8] Francis F. Chen. *Introduction to Plasma Physics and Controlled Fusion*. Springer International Publishing, Cham, 2016.

[9] Steven R. Cranmer. New views of the solar wind with the Lambert W function. *American Journal of Physics*, 72(11):1397–1403, November 2004.

[10] Roldão da Rocha. Black hole acoustics in the minimal geometric deformation of a de Laval nozzle. *The European Physical Journal C*, 77(5):355, 5 2017. [Online; accessed 2023-03-02].

[11] L. Del Zanna, M. Velli, and P. Londrillo. Dynamical response of a stellar atmosphere to pressure perturbations: numerical simulations.

[12] Hironobu Furuhashi, Yasusada Nambu, and Hiromi Saida. Simulation of an acoustic black hole in a Laval nozzle. *Class. Quantum Grav.*, 23(17):5417–5438, September 2006.

[13] J. Gaite. Perturbations in the self-similar Bondi flow. 449(3):861–868.

[14] R. Grappin, E. Cavillier, and M. Velli. Acoustic waves in isothermal winds in the vicinity of the sonic point.

[15] Seung-Yeal Ha, Taeyoung Ha, Chi-Ok Hwang, and Ho Lee. Nonlinear instability of the one-dimensional Vlasov-Yukawa system. *Journal of Mathematical Physics*, 52(3):033301, March 2011.

[16] Klaus Jockers. On the stability of the solar wind. *Sol Phys*, 3(4):603–610, April 1968.

[17] Igor D. Kaganovich, Andrei Smolyakov, Yevgeny Raitses, Eduardo Ahedo, Ioannis G. Mikellides, Benjamin Jorns, Francesco Taccogna, Renaud Gueroult, Sedina Tsikata, Anne Bourdon, Jean-Pierre Boeuf, Michael Keidar, Andrew Tasman Powis, Mario Merino, Mark Cappelli, Kentaro Hara, Johan A. Carlsson, Nathaniel J. Fisch, Pascal Chabert, Irina Schweigert, Trevor Lafleur, Konstantin Matyash, Alexander V. Khrabrov, Rod W. Boswell, and Amnon Fruchtman. Physics of E $\times$ B discharges relevant to plasma propulsion and similar technologies. *Physics of Plasmas*, 27(12):120601, 12 2020.

[18] Eric Keto. Stability and solution of the time-dependent Bondi–Parker flow. *Monthly Notices of the Royal Astronomical Society*, 493(2):2834–2840, April 2020.

[19] R. Kolman, M. Okrouhlík, A. Berezovski, D. Gabriel, J. Kopačka, and J. Plešek. B-spline based finite element method in one-dimensional discontinuous elastic wave propagation. *Applied Mathematical Modelling*, 46:382–395, June 2017.

[20] O. Koshkarov, A. I. Smolyakov, I. D. Kaganovich, and V. I. Ilgisonis. Ion sound instability driven by the ion flows. *Phys. Plasmas*, 22(5):052113, May 2015.

[21] Erwin Kreyszig. *Introductory functional analysis with applications*. Wiley, New York, 1978.

[22] Justin M Little. Performance scaling of magnetic nozzles for electric propulsion, 2015. ISBN: 9781321565317.

[23] Andrei A. Litvak and Nathaniel J. Fisch. Rayleigh instability in Hall thrusters. *Physics of Plasmas*, 11(4):1379–1383, April 2004.

[24] X. Llobet, K. Appert, A. Bondeson, and J. Vaclavik. On spectral pollution. *Computer Physics Communications*, 59(2):199–216, June 1990.

[25] Stéphane Mazouffre. Electric propulsion for satellites and spacecraft: established technologies and novel approaches. *Plasma Sources Sci. Technol.*, 25(3):033002, June 2016.

[26] Satoshi Okuzumi and Masa-aki Sakagami. Quasinormal ringing of acoustic black holes in Laval nozzles: Numerical simulations.

[27] Ivan Romadanov, Andrei Smolyakov, Yevgeny Raitses, Igor Kaganovich, Tang Tian, and Sergei Ryzhkov. Structure of nonlocal gradient-drift instabilities in Hall E × B discharges. *Physics of Plasmas*, 23(12):122111, December 2016.

[28] D. D. Ryutov, P. N. Yushmanov, D. C. Barnes, and S. V. Putvinski. Divertor for a linear fusion device. page 060003, Newport Beach, CA, USA, 2016.

[29] A. I. Smolyakov, A. Sabo, P. Yushmanov, and S. Putvinskii. On quasineutral plasma flow in the magnetic nozzle. *Physics of Plasmas*, 28(6):060701, June 2021.

[30] R. F. Stellingwerf and J. Buff. Stability of astrophysical gas flow. I - Isothermal accretion. *ApJ*, 221:661, April 1978.

[31] T. Theuns and M. David. Spherically symmetric, polytropic flow. 384:587.

[32] Satoshi Togo, Tomonori Takizuka, Dirk Reiser, Mizuki Sakamoto, Yuichi Ogawa, Naomichi Ezumi, Kenzo Ibano, Kunpei Nojiri, Yue Li, and Yousuke Nakashima. Characteristics of plasma flow profiles in a super-X-divertor-like configuration. *Nuclear Materials and Energy*, 19:149–154, May 2019.

[33] Lloyd N. (Lloyd Nicholas) Trefethen. *Spectral methods in MATLAB*. Software, environments, tools. Society for Industrial and Applied Mathematics, Philadelphia, PA, 2000.

[34] WG Unruh. Sonic analogue of black holes and the effects of high frequencies on black hole evaporation. *Physical review. D, Particles and fields*, 51(6):2827–2838, 1995.

[35] M. Velli. From supersonic winds to accretion: Comments on the stability of stellar winds and related flows. 432:L55.

[36] M. Velli. Hydrodynamics of the Solar Wind Expansion. 277(1/2):157–167.

[37] Craig H. Williams. Fusion Propulsion Through a Magnetic Nozzle and Open Divertor. In *AIP Conference Proceedings*, volume 654, pages 510–515, Albuquerque, New Mexico (USA), 2003. AIP. ISSN: 0094243X.

Appendix A

Lambert W Function

Definition 3. The Lambert W function is a function, $y(x)$, such that the following equation holds

$$ye^y = x$$

where y and x are real. The Lambert W function is denoted as $W_k(x)$, where $k = 0, -1$ are its two branches.

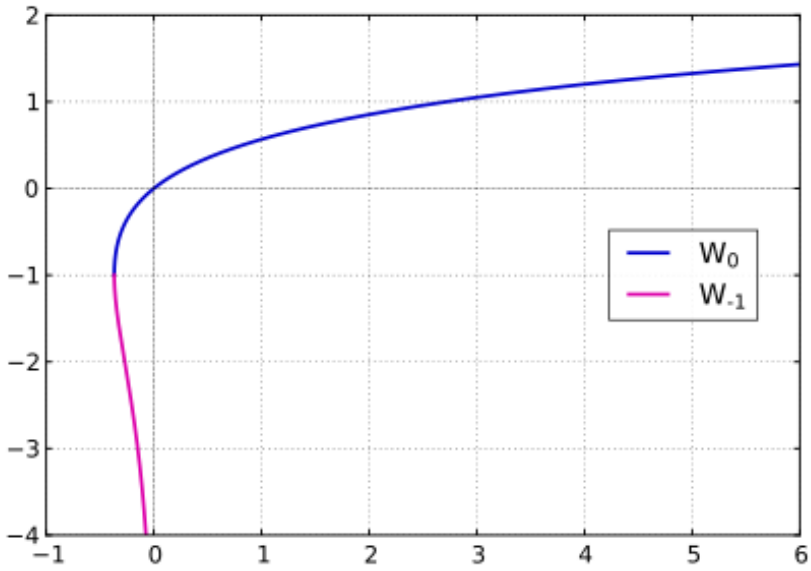

Figure A.1: The graph of $y = W(x)$ for real $x < 6$ and $y > -4$. The upper branch (blue) with $y \geq -1$ is the graph of the function $W_0(x)$ (principal branch), the lower branch (magenta) with $y \leq -1$ is the graph of the function $W_{-1}(x)$. The minimum value of x is at $(-1/e, -1)$.

Appendix B

Verification of Analytical Solutions

Theorem 3. The general solution to

$$\omega^2\tilde{v} + 2i\omega\frac{\partial\tilde{v}}{\partial z} + (1-v_0^2)\frac{\partial^2\tilde{v}}{\partial z^2} = 0$$

is

$$\tilde{v} = \exp\left(-\frac{i\omega}{v_0+1}\right)\left[\exp\left(i\omega\frac{z+1}{v_0+1}\right) - \exp\left(i\omega\frac{z+1}{v_0-1}\right)\right]$$

Proof. The derivatives of $\tilde{v}$ are

$$\begin{aligned}
\tilde{v} &= \exp\left(-\frac{i\omega}{v_0+1}\right)\left[\exp\left(i\omega\frac{z+1}{v_0+1}\right) - \exp\left(i\omega\frac{z+1}{v_0-1}\right)\right] \\
\frac{\partial\tilde{v}}{\partial z} &= i\omega\exp\left(-\frac{i\omega}{v_0+1}\right)\left[\frac{1}{v_0+1}\exp\left(i\omega\frac{z+1}{v_0+1}\right) - \frac{1}{v_0-1}\exp\left(i\omega\frac{z+1}{v_0-1}\right)\right] \\
\frac{\partial^2\tilde{v}}{\partial z^2} &= -\omega^2\exp\left(-\frac{i\omega}{v_0+1}\right)\left[\frac{1}{(v_0+1)^2}\exp\left(i\omega\frac{z+1}{v_0+1}\right) - \frac{1}{(v_0-1)^2}\exp\left(i\omega\frac{z+1}{v_0-1}\right)\right]
\end{aligned}$$

Then the rest is easy,

$$\begin{aligned}
&\omega^2\tilde{v} + 2i\omega\frac{\partial\tilde{v}}{\partial z} + (1-v_0^2)\frac{\partial^2\tilde{v}}{\partial z^2} \\
=&\exp\left(-\frac{i\omega}{v_0+1}\right)\left(1 - \frac{2v_0}{v_0+1} + \frac{(1-v_0^2)}{(v_0+1)^2}\right)\exp\left(i\omega\frac{z+1}{v_0+1}\right) \\
&- \exp\left(-\frac{i\omega}{v_0+1}\right)\left(1 - \frac{2v_0}{v_0-1} + \frac{(1-v_0^2)}{(v_0-1)^2}\right)\exp\left(i\omega\frac{z+1}{v_0-1}\right) \\
=&0
\end{aligned}$$

□

Theorem 4. If $\omega = n\pi(1 - v_0^2)/2$, then $\tilde{v}(\pm 1) = 0$.

Proof. It is easy to see that $v(-1) = 0$. As for $z = 1$, we have

$$\begin{aligned}
\tilde{v}(1) &\propto \exp\left(\frac{2i\omega}{v_0 + 1}\right) - \exp\left(\frac{2i\omega}{v_0 - 1}\right) \\
&= \exp(in\pi(1 - v_0)) - \exp(-in\pi(1 + v_0)) \\
&= (-1)^n \exp(-in\pi v_0) - (-1)^n \exp(-in\pi v_0) \\
&= 0
\end{aligned}$$

□

Theorem 5. If

$$\omega = (v_0^2 - 1)\left[\frac{n\pi}{2} - \frac{1}{4} i \ln\left(\frac{v_0 - 1}{v_0 + 1}\right)\right]$$

then $\tilde{v}(-1) = 0$ and $\partial_z \tilde{v}(1) = 0$.

Proof. It is easy to see that $v(-1) = 0$. The derivative at $z = 1$ is

$$\begin{aligned}
\left.\frac{\partial \tilde{v}}{\partial z}\right|_{z=1} \propto& \frac{1}{v_0 + 1} \exp\left(\frac{2i\omega}{v_0 + 1}\right) - \frac{1}{v_0 - 1} \exp\left(\frac{2i\omega}{v_0 - 1}\right) \\
=& \frac{1}{v_0 + 1} \exp\left(in\pi(v_0 - 1) + \frac{v_0 - 1}{2} \ln\left(\frac{v_0 - 1}{v_0 + 1}\right)\right) \\
& - \frac{1}{v_0 - 1} \exp\left(in\pi(v_0 + 1) + \frac{v_0 + 1}{2} \ln\left(\frac{v_0 - 1}{v_0 + 1}\right)\right) \\
=& \frac{(-1)^n}{v_0 + 1} \exp(in\pi v_0) \left(\frac{v_0 - 1}{v_0 + 1}\right)^{(v_0 - 1)/2} \\
& - \frac{(-1)^n}{v_0 - 1} \exp(in\pi v_0) \left(\frac{v_0 - 1}{v_0 + 1}\right)^{(v_0 + 1)/2} \\
=& 0
\end{aligned}$$

The last equality holds because

$$\frac{1}{v_0 - 1} \left(\frac{v_0 - 1}{v_0 + 1}\right)^{(v_0 + 1)/2} = \frac{1}{v_0 + 1} \left(\frac{v_0 - 1}{v_0 + 1}\right)^{(v_0 - 1)/2}$$

□